

Reprocessing of SISMAR refraction lines

Report of the SISMAR Refraction Line Project (belonging to the Plate Tectonics Modeling Project) for inclusion in the Offshore Petroleum Play Fairway Analysis

By Jean-Claude Sibuet¹ and Stéphane Rouzo²

¹Association Biogéosciences, 44 rue du Cloître, 29280 Plouzané, France
Home: (33) 2 98 48 45 20; Mobile: (33) 6 62 12 45 20; jean.claude.sibuet@gmail.com

²SRC, 6 rue des Mouettes, 29280 Plouzané, France
Home: (33) 2 98 38 21 22; srouzo@libertysurf.fr

July 31, 2010

Executive Summary

The seismic data collected during the SISMAR survey on the Atlantic margin off Morocco in 2001 (Contrucci et al., 2004) reveal a transitional crust difficult to interpret. The existence of a new wide-angle seismic profile on the conjugate margin of Nova Scotia (OETR2009) and a new interpretation of the multi-channel seismic data along SISMAR profiles (Maillard et al., 2006) put forward the importance of a new modeling of the SISMAR wide-angle data, with ocean instruments properly relocated and using a different approach. Contrary to the initial modeling, in which a trial and error approach has been used to constrain a layered velocity model (*rayinvr*, Zelt and Smith, 1992), the present study is based on the tomographic approach, which provides a smoothly varying velocity model and requires much less *a priori* information. Korenaga's *tomo2d* (2000) inverts jointly P-wave travel times of seismic rays refracted in the crust and mantle, and reflected at the base of the crust, thus constraining velocities in the crust and mantle and the depth of the reflector at the base of the crust. Different tests are carried out to better estimate the strength of the final model.

The velocities obtained show that along the main profile, the transitional crust features a positive velocity anomaly (serpentinized mantle velocities at the base of the transitional crust) located below the S1 magnetic anomaly, that was not visible in the Contrucci et al. (2004) modeling. In addition, the shape of layers given by Contrucci et al. (2004) does not reflect the existence of a major detachment fault (LDR) on MCS profiles. From our proposed tomographic velocity model we suggest: 1) the continental crust thins from the shelf to OBH09 and then progressively disappears from OBH09 to 12, above the LDR identified on MCS profiles and in the tomographic velocity model. 2) below the extremely thin upper plate, the lower plate consists of serpentinized mantle probably overlain by lower crust. The relative motion along the LDR would be ~20 km. 3) the western extremity of SISMAR04 is located on the flank of Coral Patch

Seamount, suggesting that OBH13 and 14 are not representative of the crust west of magnetic anomaly S1 and do not correspond to the counterpart portion of OETR2009 Profile. However, old sonobuoy data suggest that the crust west of S1 consists of serpentinized mantle, similar to the one found on OETR2009 Profile.

On OETR2009 Profile, a 90-km long, 4-5 km thick body has been identified at the base of the crust. Velocities of 7.2 to 7.5 km/s suggest that this body is serpentinized mantle. On top of it, a 2-3 km thick layer with velocities of 5.3 km/s corresponds to a layer of highly serpentinized mantle, whose top coincides with the hummocky basement on the coincident MCS profile.

Though conjugate profiles SISMAR04 and OETR2009 are 100-km offset in plate reconstructions and the western extremity of Profile SISMAR04 is located on an abnormal feature (Coral Patch Seamount), we have proposed reconstructions of velocity profiles SISMAR04 and OETR2009 at the time of magnetic anomalies ECMA/S1 (195 Ma, latest Triassic) and E (175 Ma, Middle Jurassic, Aalenian). We suggest that the crust in between 195 and 175 Ma consists of serpentinized mantle formed by seafloor spreading for the following reasons: 1) the contact of the 6-km thick serpentinized body with the lower/upper continental crust on OETR2009 Profile is almost vertical, excluding mantle exhumation along a low angle detachment fault. 2) on SISMAR04 MCS Profile, from S1 to the flank of Coral Patch Seamount (over a distance of 110 km), the deep sediment layers regularly onlap westward on top of the basement, suggesting that the acoustic basement is younger to the west. 3) from kinematic considerations, the Central Atlantic opening is symmetrical since 195 Ma.

During the first phase of rifting (late Triassic), ending at the time of emplacement of the ECMA/S1 magnetic anomalies (195 Ma), the continental crust thinned, probably by pure shear. During the second phase of rifting (195 Ma to 175 Ma), about 20 km of lower plate was extracted from beneath the Moroccan margin, bringing the lower crust belonging to the lower plate close to the sea-bottom and then, the asthenospheric mantle raised to the sea-bottom. About 200 km of serpentinized mantle was emplaced by sea-floor spreading before the setting of typical oceanic crust 175 Ma ago.

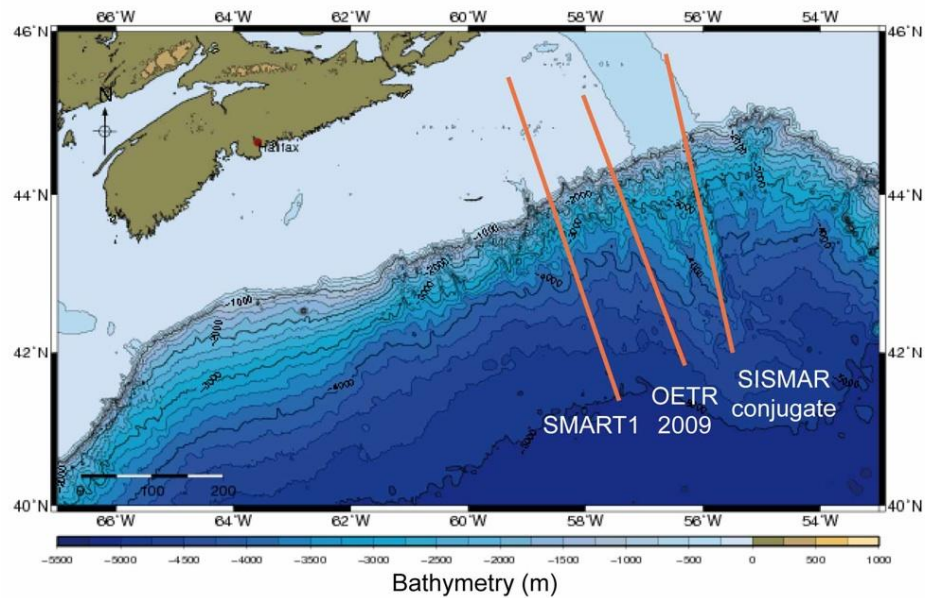
Introduction

During the Fall 2009, Geopro shot a seismic refraction line (OETR2009) off Nova Scotia, which was initially supposed to be the conjugate of the SISMAR04 line. In fact, the true conjugate line of the SISMAR04 line is located within the Newfoundland province, about 100 km northeast of Line OETR2009 (Figure 1). Preliminary results of Line OETR2009 (personal communication, Makris, 2010) and SMART01 refraction line (Funk et al., 2004), located about 100 km southwest of Line OETR2009, show very similar crustal bodies and velocities, suggesting a 2D crustal structure of the segment of Nova Scotia margin located in between these 2 profiles. It is tempting to extend this 2D crustal structure to the location of the conjugate SISMAR04 line because the trend of the margin is linear and because the East Coast Magnetic Anomaly (ECMA) is of very low amplitude beneath the 3 profiles. However, only a detailed study of multi-channel seismic (MCS) lines acquired in this area may give a clear answer concerning

the 2D structure of the margin and thus of the accuracy of conjugate velocity and structure profiles.

The SISMAR04 wide angle refraction seismic line offshore Morocco was modeled using the combined forward and inverse modeling software package rayinvr (Zelt and Smith, 1992). At the Nova Scotia Offshore Plate Reconstruction and Play Concepts Workshop (Halifax, May 11 - 13, 2009), the participants agreed that the results were difficult to interpret. It was suggested to reprocess this line by using a tomographic technique in order to try to better understand the nature of the transitional crust. We have used the joint refraction and reflection travel-time tomography method developed by Korenaga et al. [2000] to construct two-dimensional velocity models for the SISMAR profiles.

The Korenaga tomographic approach provides a smooth velocity model mostly constrained by the refracted phases. Compared to the Zelt approach, this technique requires much less *a priori* information and prevents from over-interpretating the data. To better understand the nature and geometry of the transitional crust of the Moroccan margin, it is important to compare and discuss simultaneously the final models obtained by the two methods. Finally, even if the conjugacy of the SISMAR04 and OETR2009 lines is not perfect, we will try to understand how the velocity structure across the Nova Scotia-Morocco conjugate margins might help to constrain the formation and evolution of this pairs of very old continental margins.



Magnetic Anomaly Map, BIO (2000)

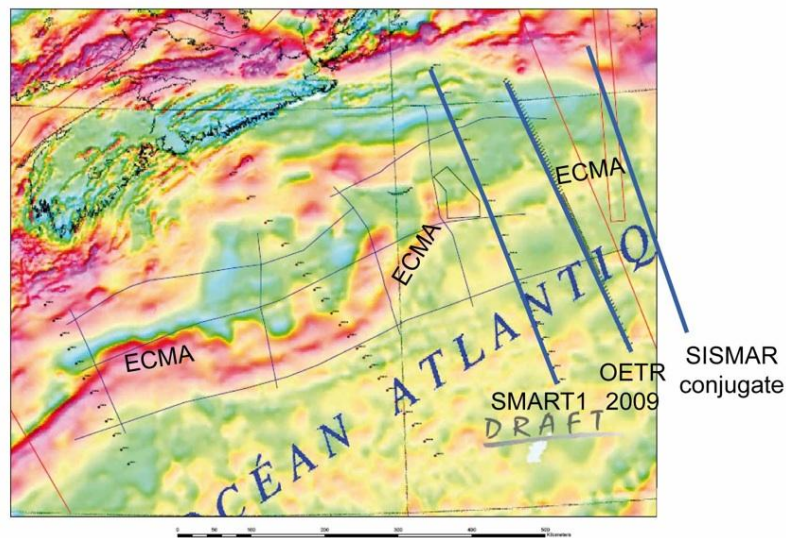


Figure 1: Location of refractions lines OETR2009, SMART01 and of the conjugate SISMAR04 line on the bathymetric and magnetic maps offshore Nova Scotia. Note that the three lines seems to belong to the same linear segment of margin and cut across the subdued portion of ECMA.

The SISMAR seismic experiment

In 2001, the SISMAR marine seismic survey acquired deep reflection seismic data as well as wide-angle seismic profiles on the Atlantic margin off Morocco. The objectives were to

image the deep structure of the margin, characterize the nature of the crust in the transitional domain and define the geometry of the synrift basins. The wide-angle seismic (WAS) reflection and refraction experiment consists in 24 ocean-bottom hydrophone (OBH) deployments and 18 land stations, along 4 shooting lines, for a total of 1000 km. The design of the experiment is shown in Figure 2 (Jaffal et al., 2009):

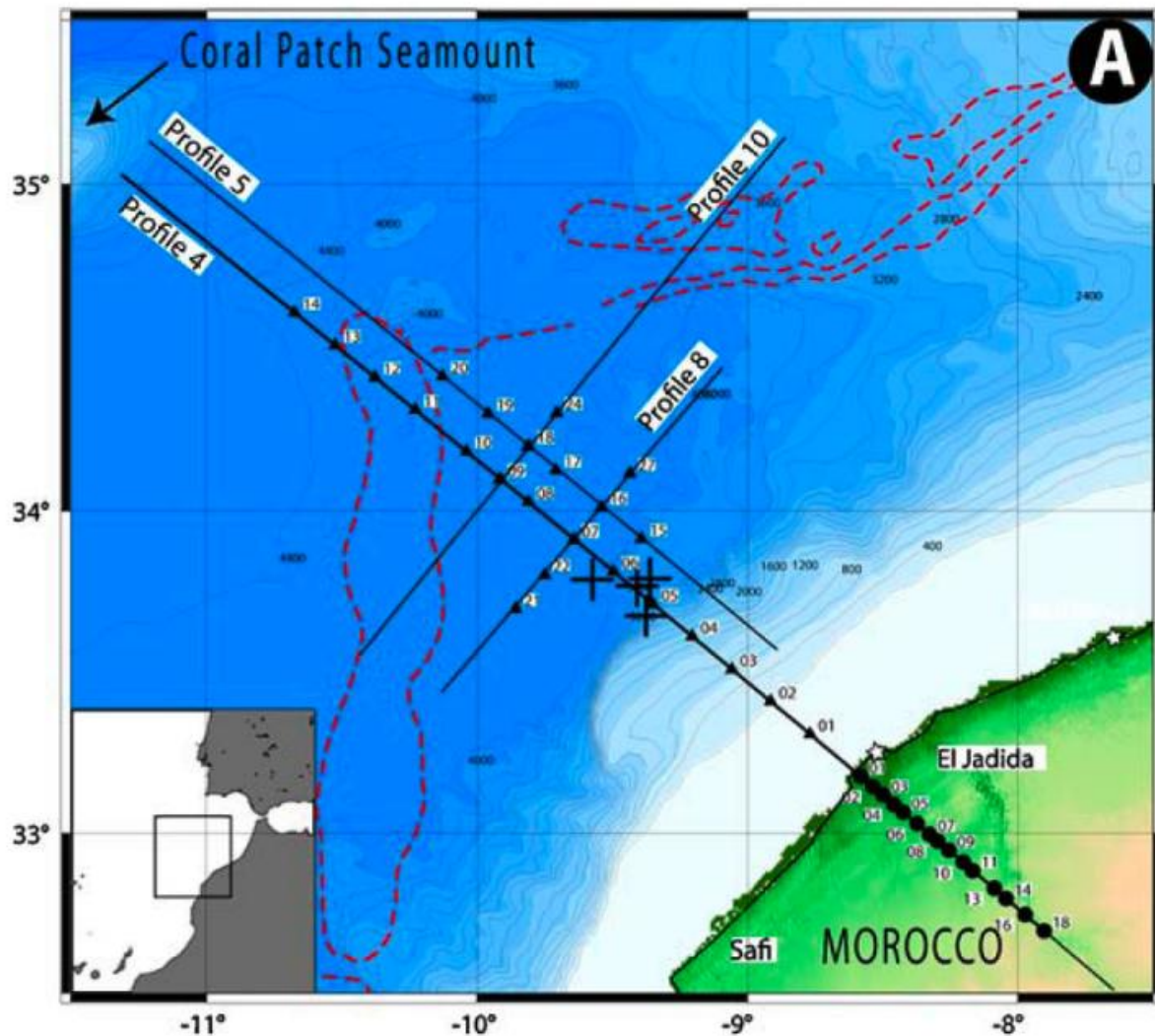


Figure 2: Location of wide-angle seismic reflection and refraction lines off Morocco. OBH positions are marked by triangles. Land stations are marked by dots. The red dashed lines underline the S1 magnetic anomaly, which is considered as the conjugate of the East Cost Magnetic anomaly. Large crosses are DSDP holes. The whole area is affected by a layer of salt in the deep sediments, which gives locally salt diapirs.

The modeling of the WAS reflection and refraction data has been published in Contrucci et al. (2004) and Jaffal et al. (2009). The layering of the sediments and the structure of the basement top benefited from the coincident MCS profiles. The four velocity profiles are displayed in Figure 3.

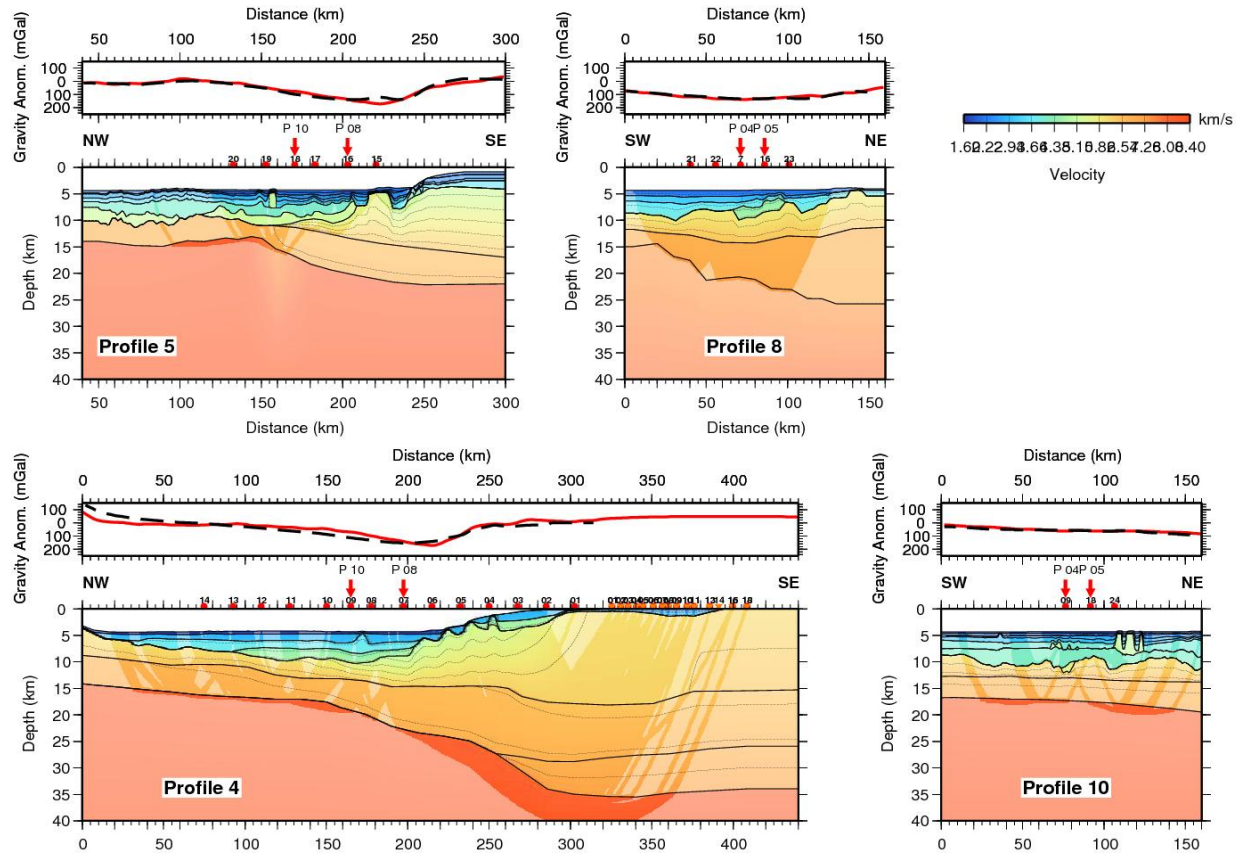


Figure 3: Final velocity models of the four SISMAR profiles (Contrucci et al., 2004; Jaffal et al., 2009), including the model boundaries (solid lines) used during inversion. Iso-velocity contours every 0.25 km/s. Darker shaded areas show ray paths (reflected or refracted) from the modeling and hence regions of the model that are constrained. Above the models, measured gravity anomalies (red lines) and anomalies predicted from the models (black dashed lines).

The interpretation of the main SISMAR04 profile (Contrucci et al., 2004) shows relatively slow velocities beneath the continental slope, with a low velocity anomaly fading away progressively below the deep sedimentary basin at the foot of the slope. The velocity distribution is compatible with an oceanic nature beneath the most seaward instrument (OBH 14). Notice that SISMAR04 Profile intersects the S1 magnetic anomaly near OBH 12 and 13. Profiles 5 and 10 are severely affected by salt diapirism and velocity models rely on a small amount of seismic rays.

Objectives of the present study and method

The present study focuses on the interpretation of the nature of the transitional crust seaward of the continental slope, where problems in the interpretation were identified during the 2009 Halifax meeting. In particular, the possible presence of exhumed continental mantle or volcanic rocks along Profile SISMAR04 as suggested by Maillard et al. (2005) is assessed. To

have a fresh sight on the velocities below the sediments, a new modeling is carried out in this study, following a tomographic approach. The interest of the tomographic approach is that it does not rely on a sophisticated interpretation of the data. The travel-time tomographic tool we use provides a smoothly varying velocity model mostly constrained by the refracted phases. Compared to the initial modeling carried out using the Zelt package, this tomographic approach requires only the identification of first arrival events and the final velocity model introduces much less *a priori* information and over-interpretation.

The 2-D tomographic tool used in this study is *tomo2d*, developed by Korenaga et al. (2000). It is actually a joint refraction and reflection travel-time tomography method. Refracted phases (first arrivals) and reflections at the base of the crust (PmP) are inverted simultaneously to provide a one-layer, continuously varying velocity model and a floating reflector representing the base of the crust. The forward modeling and most aspects of the inverse algorithm are described in Korenaga et al. (2000). Notice that the reflector at the base of the crust is not correlated to any velocity jump: it is not *stricto sensu* the Moho interface. Both the refraction and reflection travel-times constrain the velocities. The relative influence of the two sources of perturbation of velocity in the inversion process is set manually through a weighting factor w . A value of 1 is used throughout this study, giving an equal weight to both sources. However, theory and observation show that velocity variations arise mainly from the refracted data.

A starting velocity model is required by the tomographic approach. The shallower part of this model is built using the structure and velocity of the sedimentary layers inferred from the initial modeling (Contrucci et al. 2004), themselves constrained by the MCS interpretation. This "knowledge" is introduced at once, as it is not questioned by the present study. Below the basement, the velocity is reset uniformly to 6 km/s and a vertical gradient is added. Eventually, the whole starting model is filtered to remove smaller details, in order to facilitate ray tracing. The gridding scheme adopted by *tomo2d* is adapted to continental margins problems: contrary to other tomographic tools, which set the grid from the sea surface (inducing steps at the sea-bottom and crooked synthetic travel times, even for a small mesh size), the grid is hanging beneath the seafloor, which warrants this fundamental velocity interface to be accurately set. Moreover, the grid size is user-specified, and the shallower part of the model, where larger velocity gradients are expected, can be more densely sampled. Most of the models shown in this study have a 1-km horizontal mesh size, while it ranges vertically from .25 at the sea-bottom to 4 km, 40 km deeper. The starting floating reflector is introduced at a constant depth of 20 km.

Parameter values and statistics about the different experiments are listed in Table 1.

Model parameters :

Line	instruments	pick #		nodes	dimensions		grid spacing (km)	
		refrac	refl		X	Z	X	Z (0 - 40 km)
04	14 + 14	7065	2032	17892	425	40	1	.25 to 4.
04 Z	14	3997	-	23546	295	25	1	.25 to 1.
05	6	1399	0	6342	150	40	1	.25 to 4.
08	5	1399	509	6342	150	40	1	.25 to 4.
10	3	751	0	3612	85	40	1	.25 to 4.

Inversion parameters :

Line	iter.	smoothing (%)		damping(%)		correlation length (km)		χ^2		RMS (ms)	
		depth	veloc.	depth	veloc.	horiz.	vertical	initial	final	initial	final
04	10	40	15	10	50	3 to 9	0.5 to 9	114	1.07	1077	104
04 Z	6	40	15	10	50	3 to 7	0.5 to 7	54	0.94	535	71
05	9	40	15	10	50	3 to 9	0.5 to 9	10	1.04	192	61
08	9	40	15	10	50	3 to 9	0.5 to 9	22	1.2	408	88
10	10	40	15	10	50	3 to 9	0.5 to 9	10	0.97	230	73

Table 1: Model parameters and inversion parameters for the four lines of the SISMAR experiment.

OBH relocation

Relocation of OBHs consists in evaluating a more accurate position of the instruments after it has been dropped, to correct the possible drift of the instrument on its way down to the sea-bottom and up to the sea-surface. The water wave (wave travelling directly in the water from source to receiver) is picked and inverted, using the drop position as an initial guess (water velocity as well as depth of instruments are considered as reliable parameters). OBHs at the crossing of two shooting lines are relocated with more accuracy, thanks to two independent data sets.

Figure 4 shows two examples of the effect of relocating OBHs. After inversion, the “best” position on the sea-bottom can be several hundreds meters away from the drop position.

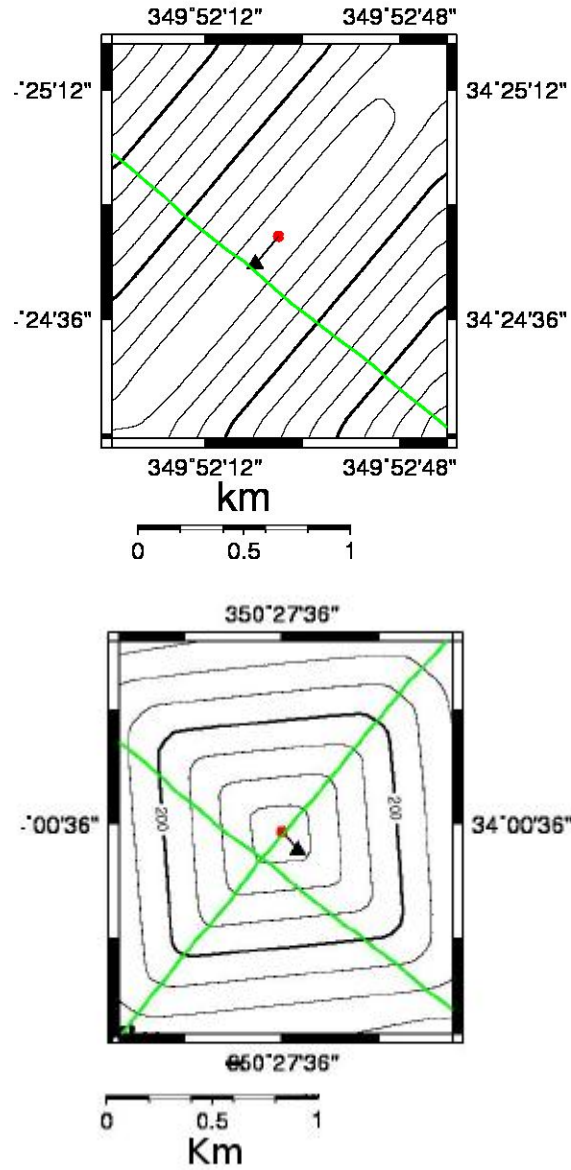


Figure 4: Relocated positions (red dots) with respect to the drop positions (black triangles) for OBH20 along SISMAR05 Line (upper panel) and OBH16 at the crossing of SISMAR05 and 08 Lines (lower panel). Green lines are shooting lines. Black curves are iso-values of the function on which the maximum is found.

OBHs along Line SISMAR04 were already relocated during the initial modeling (Contrucci et al., 2004). They are left unchanged. OBHs along Lines SISMAR05, 08 and 10 have been relocated in the present study. The more accurate positions of instruments are used to better estimate the offset (distance source-receiver). Table 2 gives the position of OBHs after relocation. The relocation process failed to estimate a reliable new position for OBH23, and its best position is assumed to be the drop position.

Line	OBS	Latitude	Longitude	Time shift (s)
5	20	34.4136009	-10.1262207	
	19	34.2997971	-9.95793056	
	18	34.1976967	-9.81063938	
	17	34.1210022	-9.71191978	
	16	34.009655	-9.53998184	
	15	33.9125023	-9.39194012	
8	23	34.1142769	-9.43446541	
	16	34.009655	-9.53998184	
	7	33.907341	-9.64333057	
	22	33.8019676	-9.75244808	
	21	33.6952477	-9.85651779	-0.63
10	24	34.3005791	-9.7058506	-0.6
	18	34.1976967	-9.81063938	
	9	34.0929	-9.91665	

Table 2: Position of OBHs after relocation.

Data quality, picking and uncertainties

The data interpretation consists in the identification and picking of the first arrival refracted and reflected events (water wave excluded). No particular processing is applied to the receiver gather prior to interpretation. The amplitude is only corrected for the increase of the offset (no AGC applied) and a gentle band-pass filter is used, so that the wave form is preserved. The picking starts from the shallower sediments and goes down to the deepest refracted events: the Pn phase, turning beneath the base of the crust, is part of the refracted phase and is carefully sought. However, the low signal to noise ratio can make the identification of this phase problematic. The reflected phase corresponds to the PmP phase, reflecting at the base of the crust. Where present, it is usually a strong amplitude event.

Note that the data have not been re-interpreted along Line SISMAR04. The picks files of the different refracted phases have simply been concatenated and edited to remove non first-arrival events. Eventually, the dataset consists in 7065 refracted and 2032 reflected travel-times. Figure 5 shows the interpretation from Contrucci et al. (2004). Deep events with an apparent velocity higher than 6 km/s can be seen up to 50 to 60 km away from the instrument.

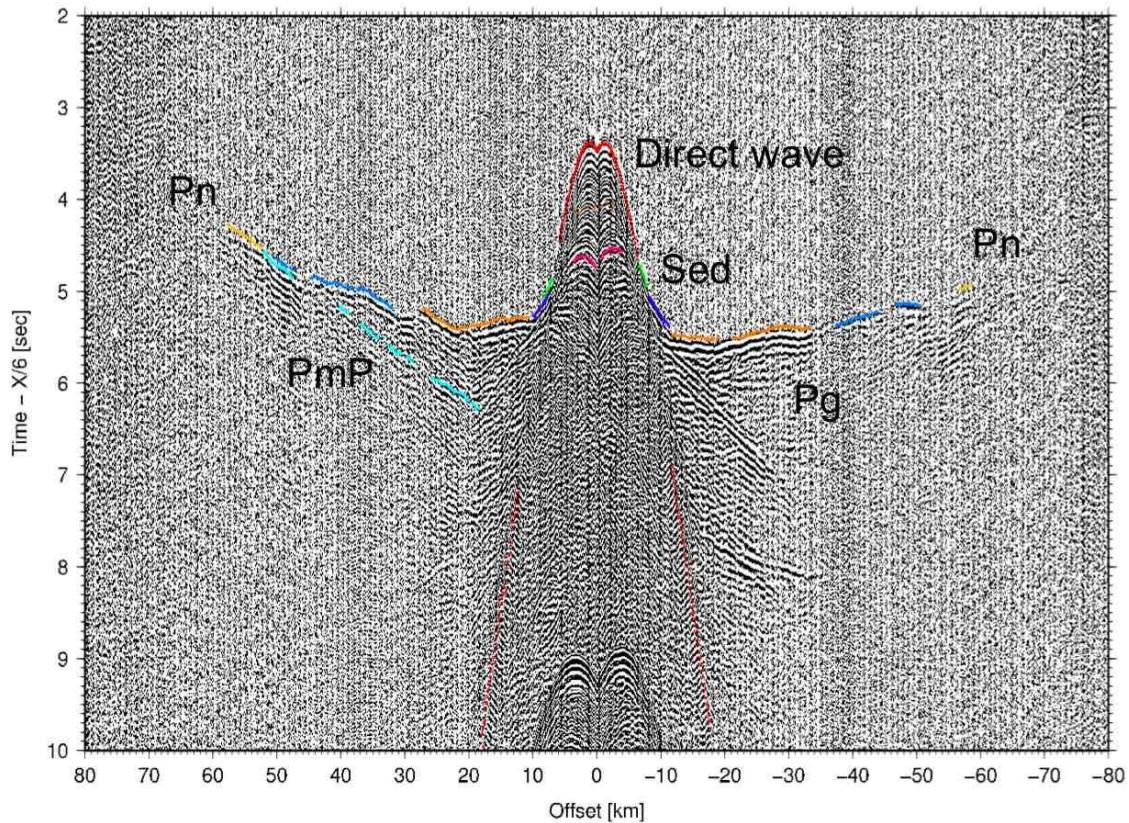


Figure 5: OBH14 on SISMAR04 Line with reduction velocity of 6 km/s. The steep red event is the water wave (1.5 km/s), sediments are green and dark blue (2 to 3 km/s), basement in orange (~ 6 km/s), lower crust in blue, Moho (Pn) in light brown. The reflected phase at the base of the crust (PmP) is in turquoise.

The quality of the record shown above is rather good. Some OBH feature disrupted events and/or maximum offsets not larger than 20 to 30 km. This poor quality of the data is likely related to the screening effect of salt diapirs. On these records, the basement top can be the deepest structure reached. The land stations provide good records and some events can be tracked up to 200 km away from the instrument. However, no event is identified seaward of the continental slope, i.e. no ray crosses the salt structures. Long and continuous PmP are easily identified and picked.

An uncertainty is ascribed to every pick. It ranges from 40 to 60 ms in the sediments, from 80 to 90 ms in the crust and is set to 110 ms for the rays reaching the mantle (Pn). As second arrivals, PmP picks have a higher uncertainty of 120 ms. Along Lines SISMAR05, 08 and 10, the “blind” picking of travel-times prevented from customizing the uncertainties depending on the depth; a constant uncertainty of 80 ms and 120 ms is set for the refracted and reflected phases respectively.

Results

SISMAR04 Profile

The complete inversion of the refracted and reflected events requires 10 iterations before the Chi2 goes down to 1. Chi2 is a statistical test that says if two populations of data are identical. A value of 1 indicates that the two populations are considered to be the same, considering the uncertainties that affect the accuracy of each value. Notice that a Chi2 between one and zero indicates that the data have been over-interpreted. The RMS is a residual time (in second) that gives the average “distance” between the observed travel-times and the synthetic travel-times. With a Chi2 close to 1, the RMS is close to the averaged uncertainty (cf. inversion parameter in Table 1).

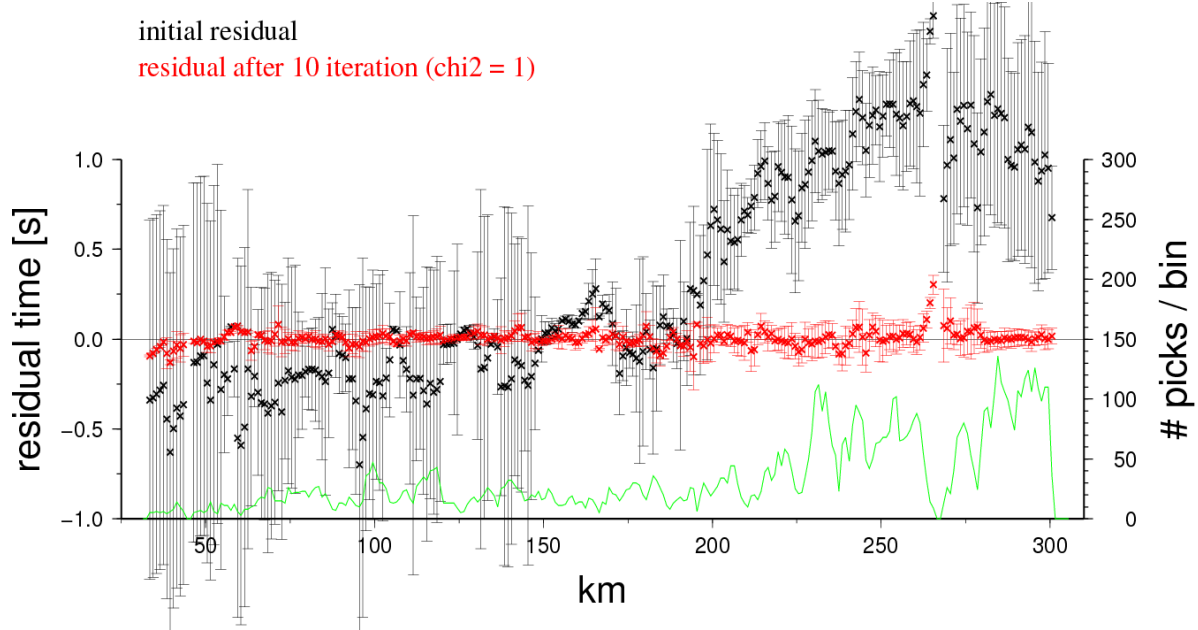


Figure 6: Residual times (observed travel-time minus synthetic travel-time) before and after inversion (in black and red respectively), according to the offset of records. The mean and standard deviations of the residual times are estimated along the shooting line within 1 km-wide bins. The green curve gives the amount of data in each bin.

Figure 6 shows that the initial residuals (black crosses) are negative for $x < 200$ km and positive for $x > 200$ km, suggesting that the starting model is on the average too slow for $x < 200$ km and too fast beyond. 200 km roughly corresponds to the foot of the continental slope. After inversion, the residual times are close to zero and feature a low variability. The event at 265 km points out that locally the inversion fails to account for the observation; it may originate from a small scale velocity structure that the inversion cannot render. It may alternatively come from the misinterpretation of part of a seismogram. Notice that very few travel-times are involved.

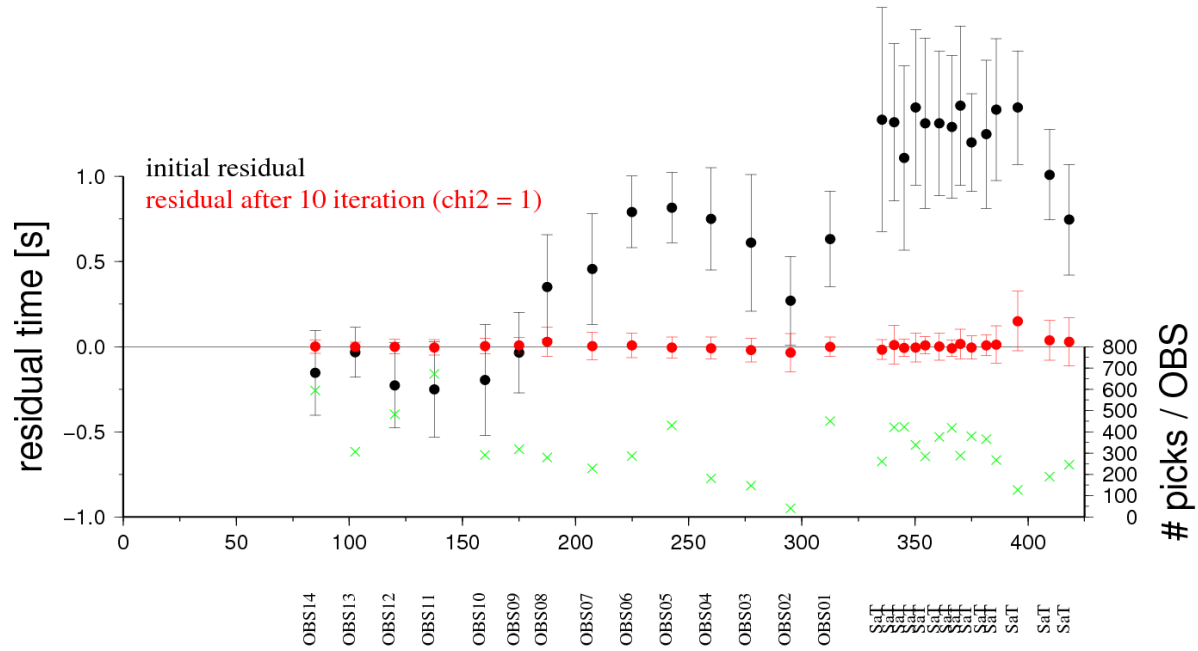


Figure 7: Residual times after inversion according to the receivers (OBHs and land stations).

In Figure 7, one simply checks that the inversion achieves a residual close to zero for each receiver (no bias on any instrument). The velocity model resulting from the inversion is shown in Figure 8. One can see the areas where the fit to the travel-times modifies the starting model.

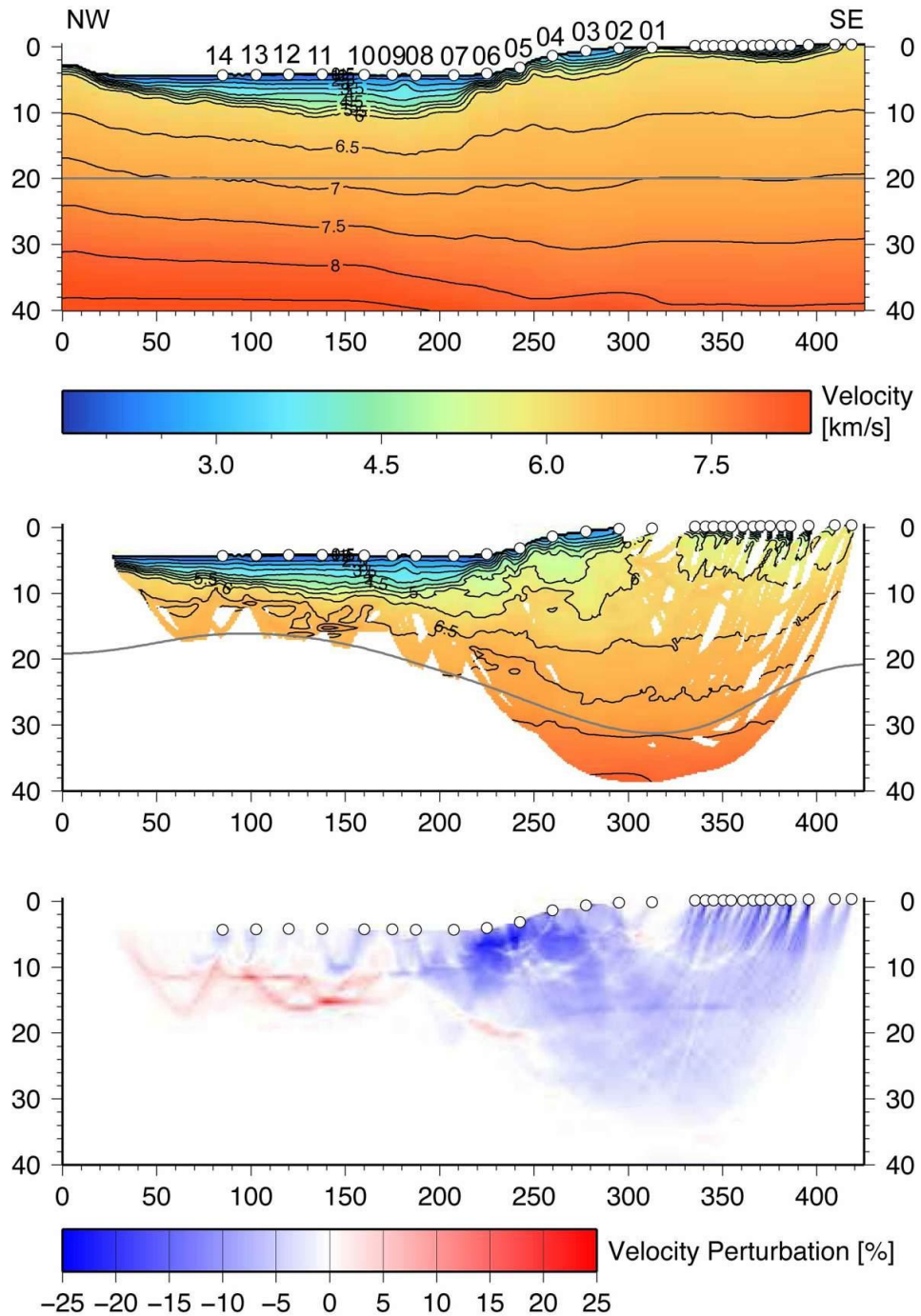


Figure 8: Starting model (top), final model (middle) and difference between the final and initial models (bottom). White circles at the surface are the OBH and land stations. The gray line is the reflector at the base of the crust.

The bottom panel (Figure 8) confirms that the starting model is too fast in the continental crust and too slow in the transitional to oceanic crust (the continental crust comes mostly in blue, while the crust is in red for $X < 180$ km).

Two observations arise from the inversion:

1) The basement velocity below the continental slope is as low as 5 km/s. The 5 km/s basement may extend eastward to the onshore part of the profile.

2) While the transitional-to-oceanic crust has a velocity of 6 to 6.5 km/s, a 7 to 7.5 km/s anomaly is visible at $x \sim 140$ km, below OBH 11. West of OBH12 ($x < 120$ km), the 6.5 km/s velocity curve is nearly horizontal at 11 km depth, whereas the velocity remains lower than 6.5 km/s down to 14 km depth from $140 \text{ km} < x < 175$ km (roughly from OBH09 to OBH11). The 7.5 km/s velocity anomaly is observed right below ($z \sim 15$ km), but it extends on about 25 km horizontally, apart from OBH11. Between this anomaly and the foot of the continental slope ($170 \text{ km} < x < 190$ km), the velocity may not be very well constrained.

The depth of the base of the crust ranges from 16 to 31 km after inversion. The shallowest point is at $x \sim 110$ km and the deepest at $x \sim 320$ km. This reflector rises up oceanward much beyond the foot of the continental slope.

Velocity inversions are visible in the final model; they are not supported by any seismic data. The downward decrease of the velocity simply reflects the return to the background velocity, which is used (and slightly changed) to invert the PmP reflection. An experiment with a starting model featuring higher velocities at these depth shows no velocity inversion. These unsupported velocity inversions are a drawback of the Pg-Pn and PmP joint inversion, in which the contribution of the reflections to the velocity constrain is weak.

The 2 to 3 km gap between the 7.5 km/s anomaly and the depth of the reflector below are significant at 15 km depth, and one cannot merge these two events in one (same origin). With a more realistic velocity between the anomaly and the reflector (i.e. velocities about 7.5 km/s) the inversion would set the reflector even deeper.

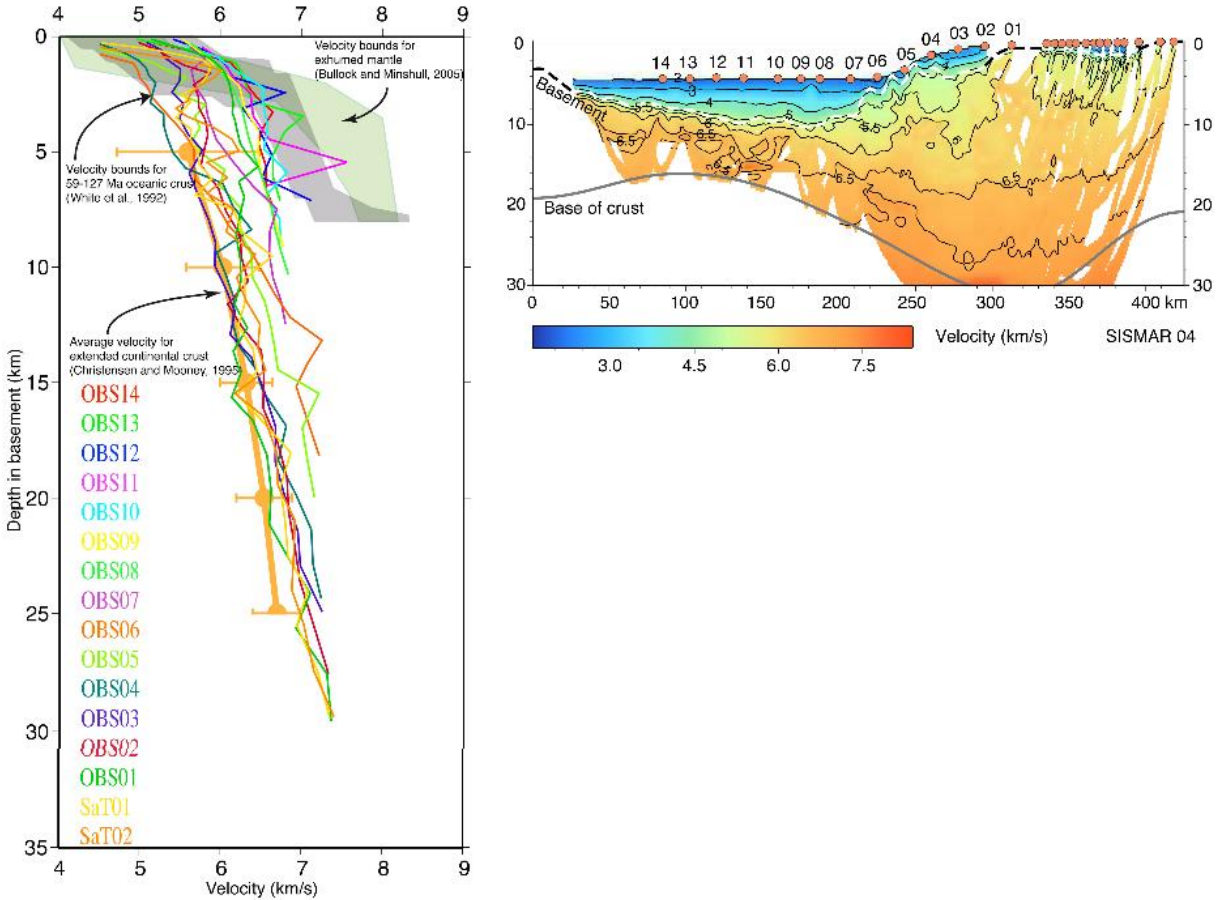


Figure 9: Final model (right panel) and 1-D vertical velocity profiles below each OBH (continuous curves of various colors). The vertical axis indicates the depth below the top-basement, defined on the MCS profile. The downward extent of the profile is bounded by the depth of the base-of-the-crust reflector. The thick orange line with error bars is the average velocity profile in extended continental crust (Christensen et Mooney, 1995). The gray and green shaded areas are the envelopes of 1-D velocity profiles in 60-to-130 Ma oceanic crust (White et al., 1992) and in exhumed mantle (Bullock and Minshull, 2005), respectively.

In Figure 9 is shown a reproduction of the final model (right panel) together with the 1-D vertical velocity profiles extracted below each instrument (left panel). When compared to trial-and-error, Zelt inferred velocity profiles (Figure 10, left panel), the tomographic-based velocity profiles (right panel) are quite rough and sometimes spiky. It actually reflects the difference between what is required in the velocity model (tomographic approach) and what is required and interpreted by a geologist eye (modeling by hand). The point is simply to highlight the interpretation contribution inherent to the trial-and-error approach.

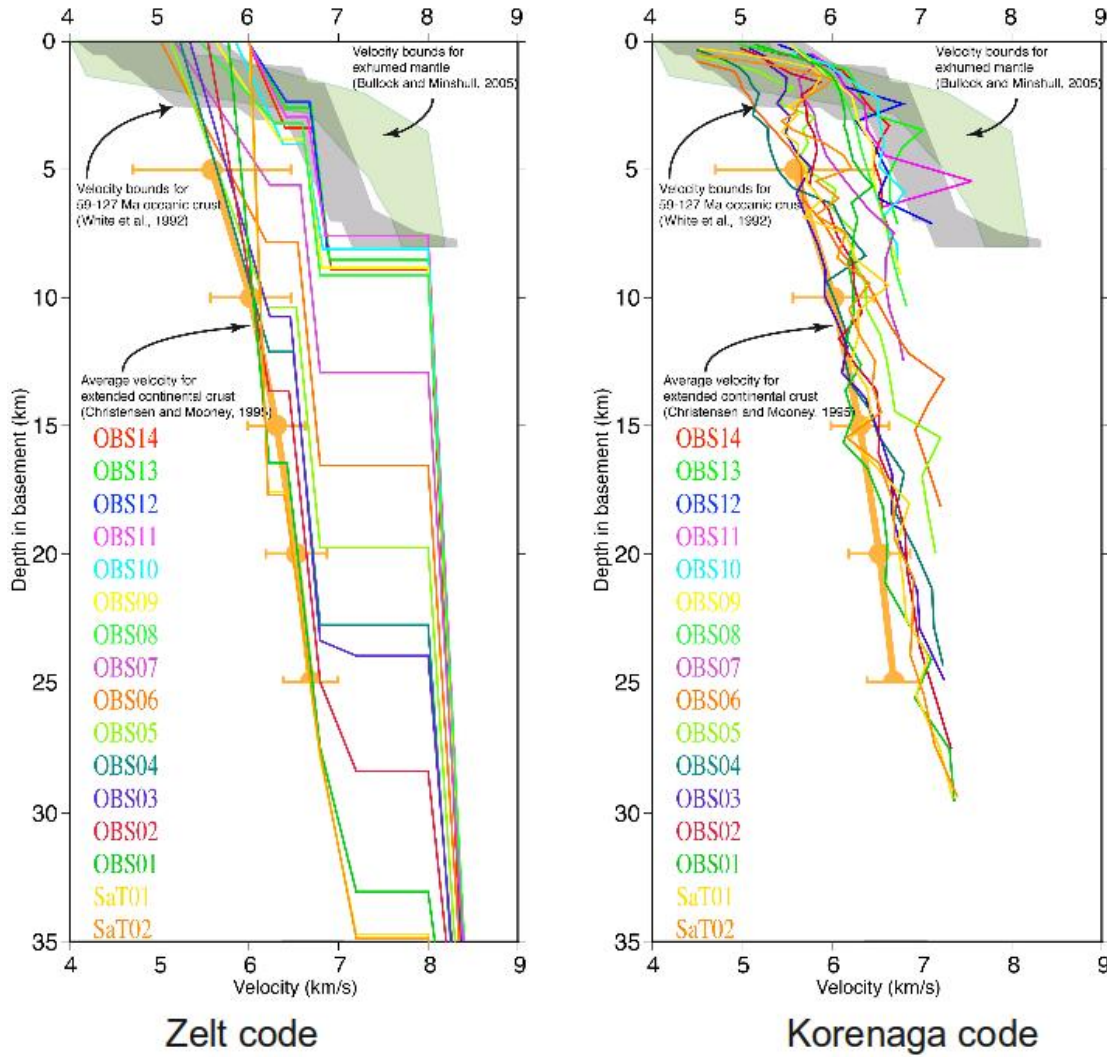


Figure 10: 1-D vertical velocity profiles below each OBH (continuous curves of various colors) when using the Zelt and Korenaga codes. The vertical axis indicates the depth below the top-basement, defined on the MCS profile.

The broken line aspect of velocity profiles reflects the paradigm on which Zelt code *Rayinvr* is based (linearly varying velocities within layers and strong velocity jumps occurring at the interface between two layers) and the grid mesh used in the tomographic experiment (velocities are continuously varying). The ~ 7.5 km/s spike of the violet curve (OBH11, right panel) observed at $z = 5$ km corresponds to the positive velocity anomaly observed in the model. The decrease of the velocity below 5 km is not supported by refraction data. It rather shows the background, not perturbed velocity that has been used to estimate the depth of the reflector (no velocity inversion supported by seismic data).

Additional tests

A set of test experiments have been run to better evaluate the strength of the tomographic model. First, different starting models have been used, to assess the sensitivity of inversion. Using the same set of inversion parameters, the final models all feature a similar

velocity distribution west of the continental slope (experiments not shown). Differences show up below the land stations, where the upper crust is poorly constrained and where the reflector is deeper than the deepest refracted phase: there, the inversion process picks the background (starting) velocity without modifying it significantly (inverting reflections alone is not efficient to improve the velocity model). The velocity inversions can be erased in tuning an *ad hoc* starting model ("ocean-like" velocity distribution), while the depth of the reflector is not significantly changed. Thus, the joint inversion of the base-of-the-crust reflector is removed in the following experiments, and the study focus on the velocities. Figure 11 (top panel) shows the velocity model after inversion of the refracted phase only, using the same inversion parameters and starting model as in the first experiment (cf. Figure 8). The only difference is the absence of velocity inversion.

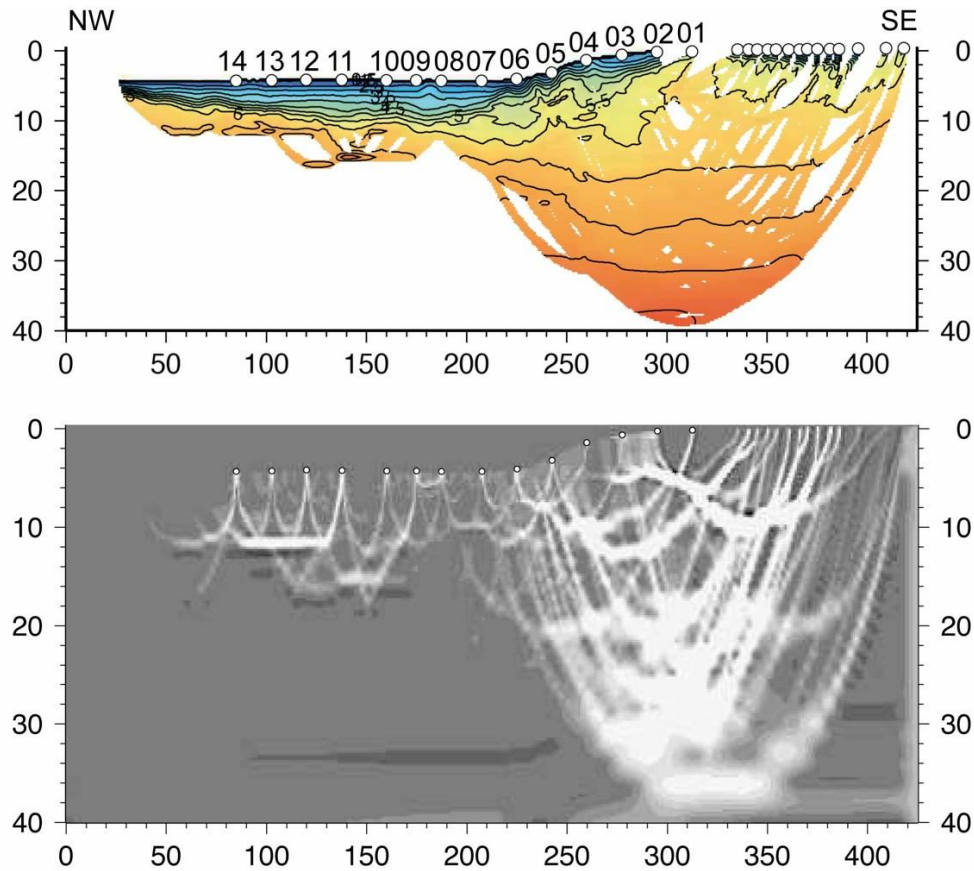


Figure 11: Derivative weight sum (bottom) of the final velocity model (top) (no wide-angle reflections inverted).

The derivative weight sum shown in Figure 11 (bottom panel) provides a qualitative representation of the ray coverage. It can be interpreted as the density of ray per cell. The white zones are the areas crossed by a large amount of rays, in which the velocity should be well constrained. It reveals that the crust between 170 and 210 km is sparsely covered, implying a lower resolution. The large white zone deep in the continental crust likely reflects the larger grid cell.

As we focus the interpretation on the transitional crust, a new experiment called Zoom (and noted as 04 Z in Table 1) has been run by using only the marine OBH stations. Land stations' records are left aside since no event has been picked westward of the foot of the slope ($x < 200$ km). Thus, the extend of the model is limited horizontally to the offshore part of the previous model, and vertically to the depth of 25 km. To improve the resolution, the griding is refined vertically (see Table 1) and the uncertainties are reduced to force the inversion to better tie to the data. In particular, the Pn uncertainty is set to 90 ms instead of 110 ms, the starting model being unchanged.

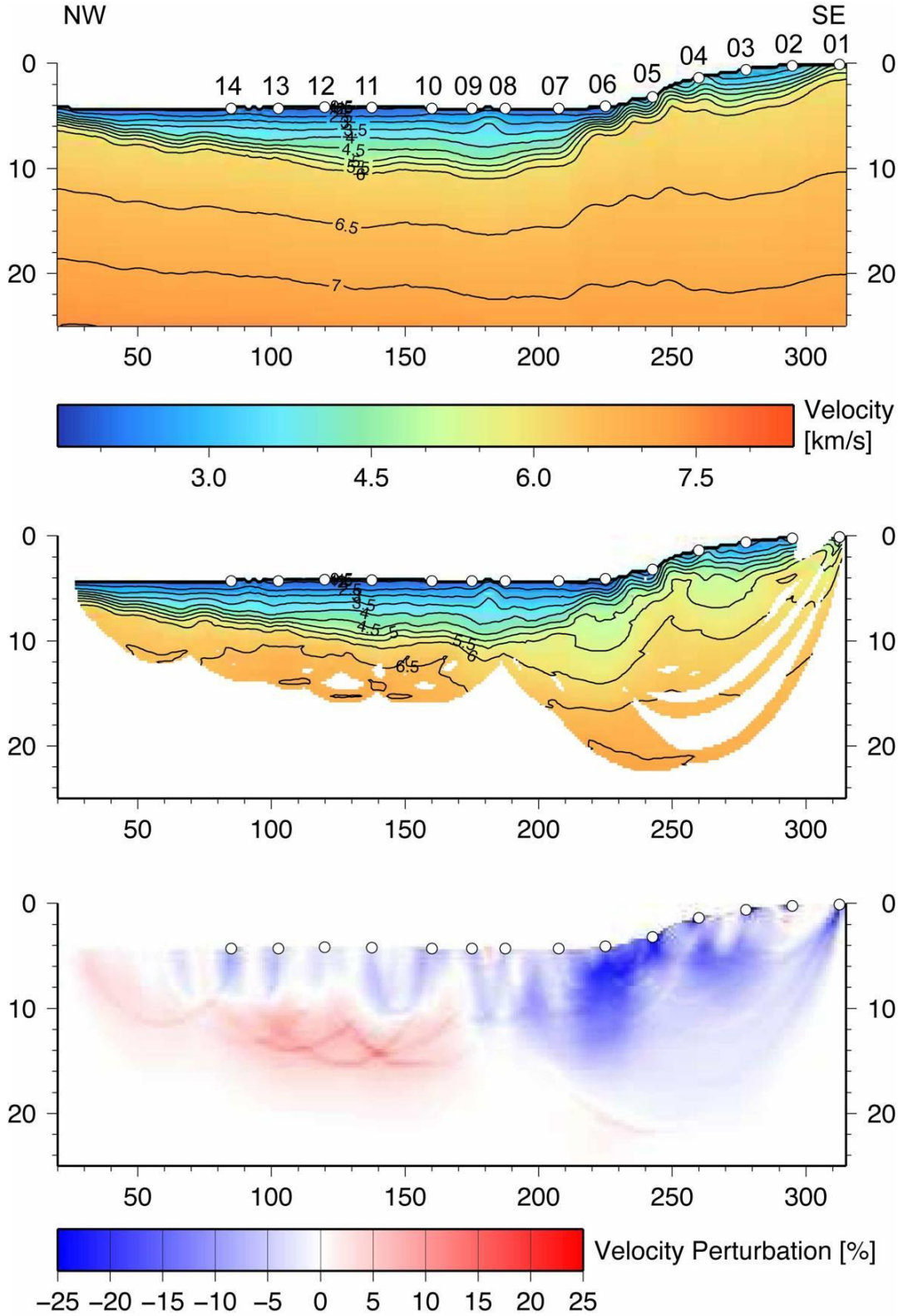


Figure 12: Zoom experiment: starting model (top), final model (middle) and difference between the final and initial models (bottom). White circles at the surface are the OBH and land stations. See Table 1 for parameters (Line 04 Z).

The positive velocity anomaly below OBH 11 now spreads between $110 \text{ km} < x < 150 \text{ km}$ while its amplitude is reduced to $\sim 7 \text{ km/s}$. One can see the effect of the finer velocity sampling in damping the anomaly. The 1-D velocity profiles (Figure 14) extracted from this experiment show a slightly different velocity distribution than in Figure 9. The positive velocity anomaly is still higher beneath OBH 11, but now it clearly spans beneath OBH 11 to 13. Compared to the meshing of the initial experiment (see Figures 8 and 9), this anomaly involves several grid points, which gives a more reliable signal: with a finer grid mesh, the velocity anomaly can extend over a larger number of points according to the ray paths and its amplitude is slightly reduced (7.15 km/s).

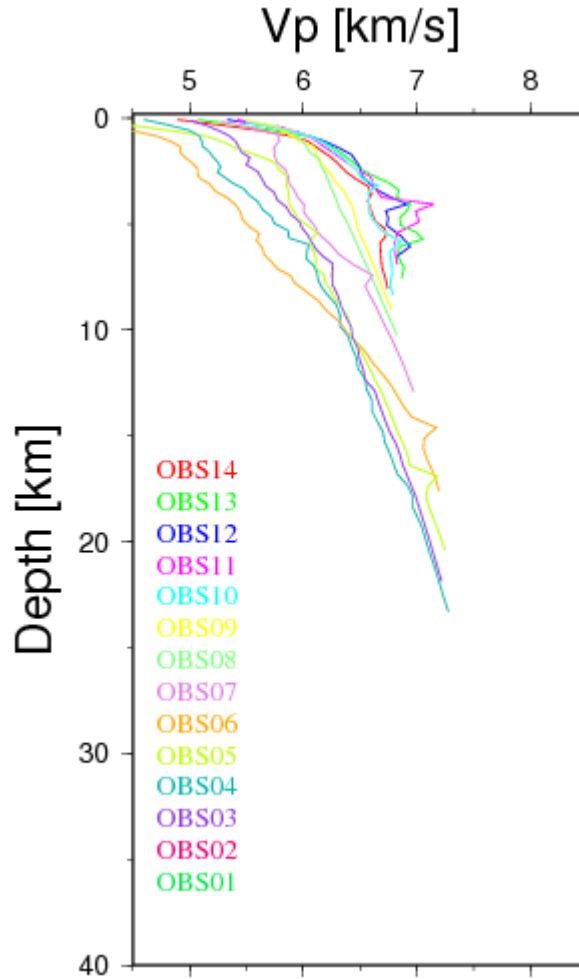


Figure 13: 1-D vertical velocity profiles below each OBH (continuous curves of various colors). The vertical axis indicates the depth below the top-basement, defined on the MCS profile.

The **spatial resolution** of the model shown in Figure 12 is assessed through a checkerboard test. This test aims at evaluating the ability of the acquisition set-up (geometry setting and data interpretation) to distinguish and constrain small velocity variations. A periodic anomaly is added to the starting model (5% amplitude) and synthetic travel-times are estimated, using the same geometry as the real experiment. A random noise of at most 100 ms is added to

these travel-times before they are inverted using the same parameters (smoothing, damping, ...) as previously.

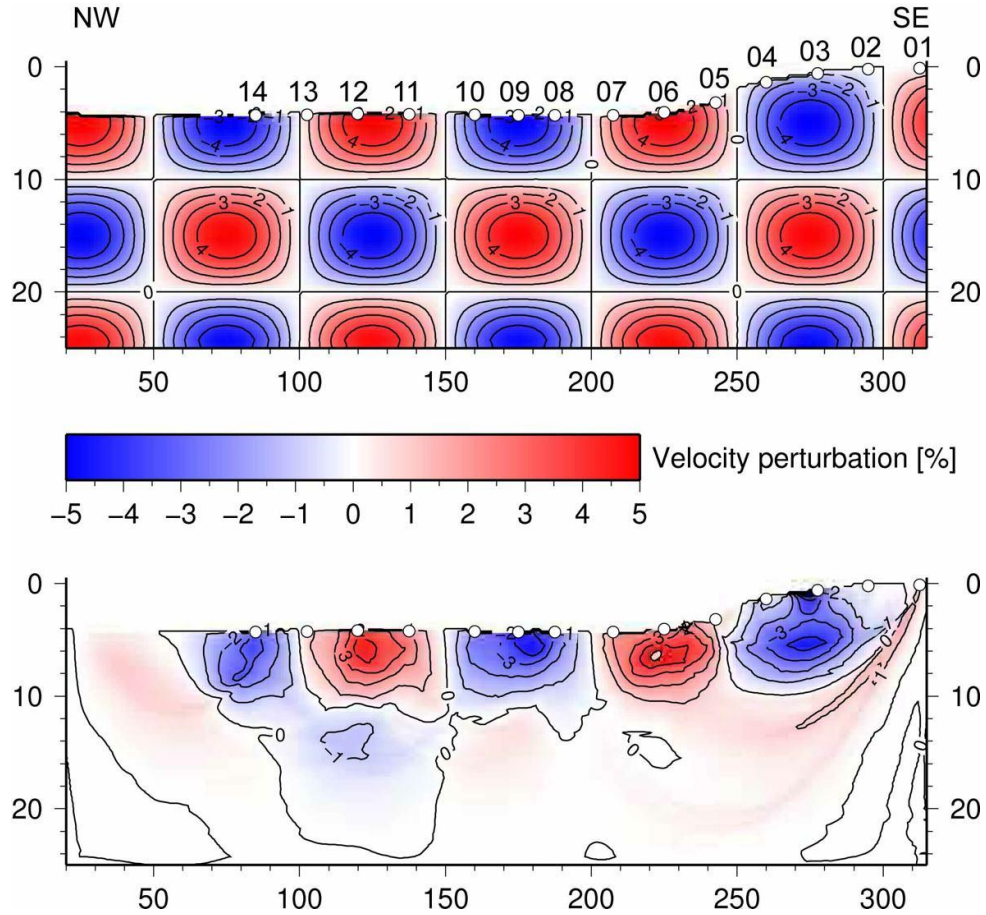


Figure 14: Checkerboard pattern of the velocity perturbation used to produce the synthetic dataset (top) and the recovered pattern after inversion (bottom) after two iterations. The tiles of the perturbation are $50 \times 10 \text{ km}^2$.

Figure 14 shows the checkerboard test applied to the experiment shown in Figure 12 (Zoom). The wavelength of the perturbation is 100 km horizontally and 20 km vertically (each tile of the perturbation pattern is $50 \times 10 \text{ km}^2$). Using the same parameters set (see Table 1), two iterations are needed for the χ^2 to be lower than unity. The checkerboard pattern as well as the amplitude are well recovered down to 10 km depth all along the profile. Below, no signal is discernible but the negative perturbation beneath OBH12 ($x \sim 120 \text{ km}$).

Figures 15 and 16 show similar experiments but with smaller perturbation patterns ($60 \text{ km} \times 10 \text{ km}$ and $40 \text{ km} \times 6 \text{ km}$ respectively).

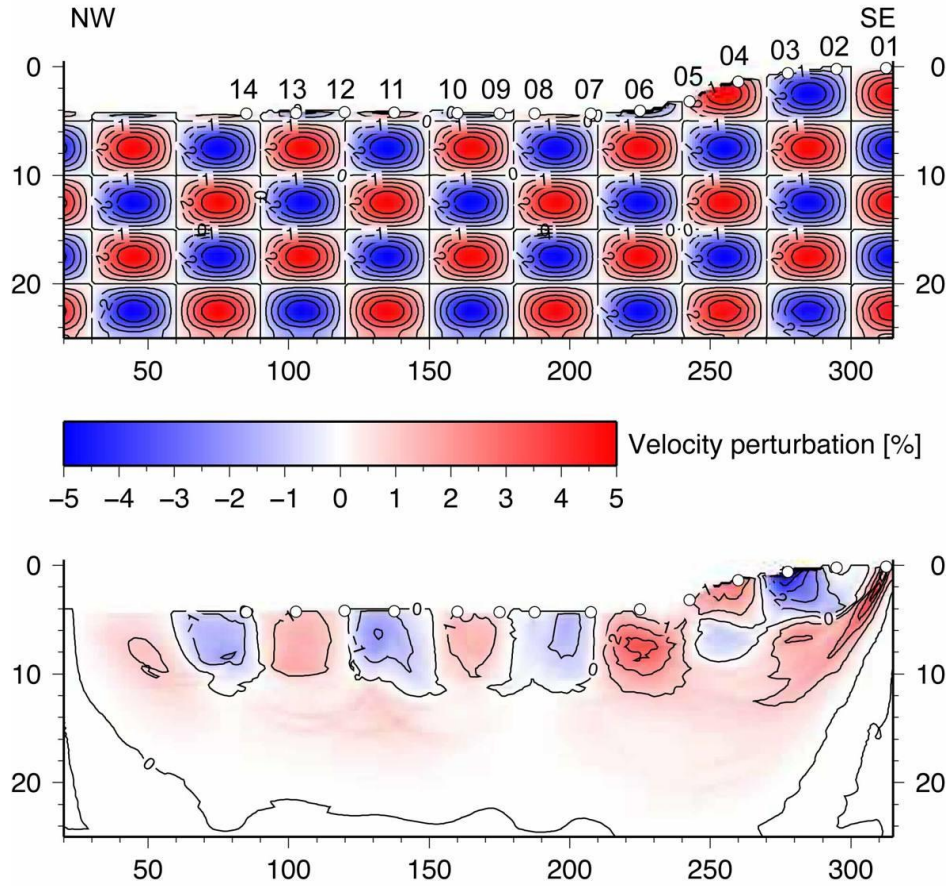


Figure 15: Checkerboard test applied to the Zoom experiment (cf. Figure 12) with a $60 \times 10 \text{ km}^2$ perturbation pattern. Bottom, recovery after 2 iterations. See comments in Figure 14.

With the $60 \times 10 \text{ km}^2$ perturbation (Fig. 15), the first row of tiles is relatively well recovered all along the profile, although the amplitude remains too weak. 5 km deeper, the pattern is nowhere visible, but the amplitudes below 10 km are found higher beneath OBH 11 and 12 (x~130 km).

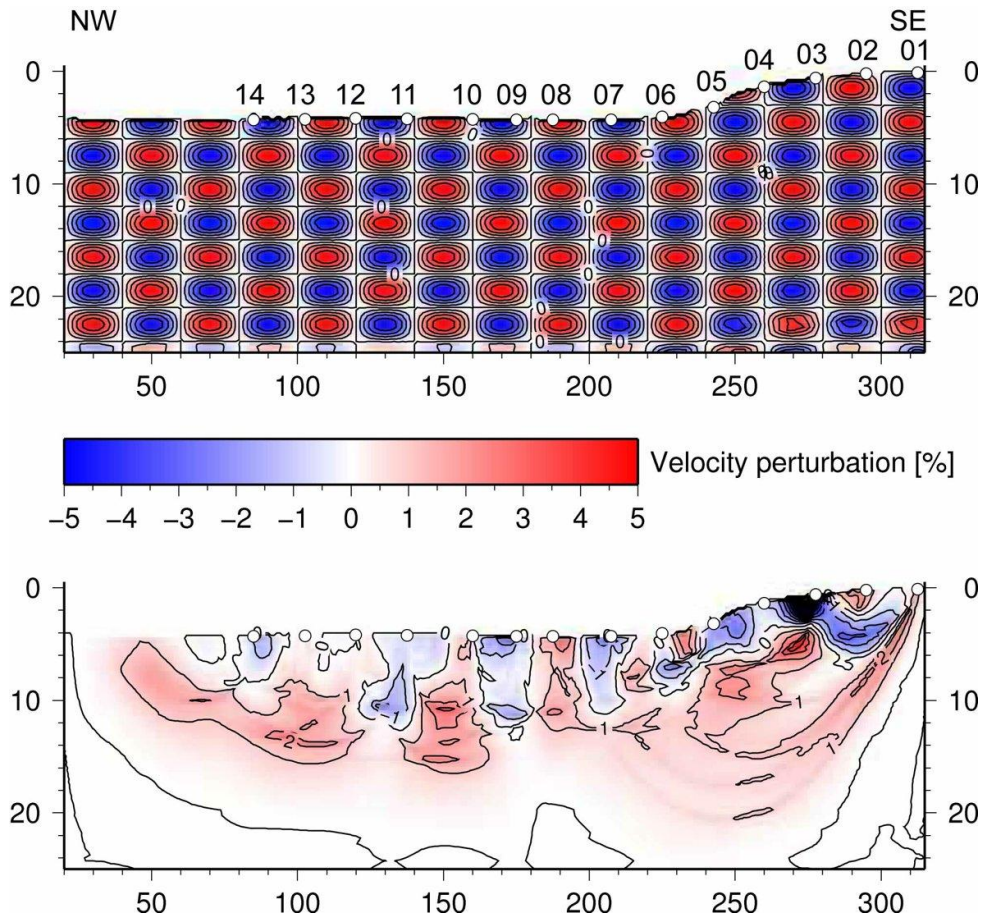


Figure 16: Checkerboard test applied to the Zoom experiment (cf. Figure 12) with a $40 \times 6 \text{ km}^2$ perturbation pattern. Bottom, recovery after 5 iterations. See comments in Figure 14.

If the perturbation pattern is set to 40 km horizontally and 6 km vertically, the recovery is poor even in the first km below the sea-floor: the pattern is hardly discernible, which means that such a small perturbation cannot be correctly resolved through this inversion setup.

These three experiments suggest that velocity anomalies larger than $30 \times 5 \text{ km}^2$ are properly constrained in size and amplitude in the 10 first km below the sea-floor. Below, the spatial resolution is low but seems slightly better for $120 < x < 150 \text{ km}$. Considering the positive velocity anomaly at $z \sim 15 \text{ km}$ below OBH 11 and 12, this resolution test suggests that its amplitude and extension are poorly constrained and one cannot rule out that it could originate from the crust-mantle interface rather than from a focused source.

Why is the mantle ($V_p = 8 \text{ km/s}$) absent from the models?

- while the Pn are quite ubiquitous on land stations' records, the OBH data provide few clear Pn events (consequence of the sub-screen imaging ?).
- Pn originating from the land stations are relatively weak constraints on velocity because the velocity in the crust is not well constrained, thus leaving the freedom to the inversion to dilute the travel-time perturbation along the long ray paths (large offsets and no shot onshore).
- Pn phases recorded on OBH are rather short. Combined to a large uncertainty and processed with smoothness as a rule, they induce a restricted velocity anomaly of limited amplitude.

In the "Zoom" experiment (see Figure 12), the Pn uncertainty is reduced to 90 ms and the mesh is finer. One observes that the positive velocity anomaly is more largely spread beneath OBH 13 to 11 while its amplitude remains higher than 7 km/s. Thus, forcing a closer fit to the data reveals a wider anomaly.

SISMAR05, 08 and 10 Profiles

Respectively 6, 5 and 3 OBHs were deployed on the three SISMAR profiles 05, 08 and 10 located in Figure 2. All the OBHs were relocated (Table 2) and the same processing procedure used for Profile SISMAR04 was applied to the three profiles. Figures 15 to 18 show the final velocity models.

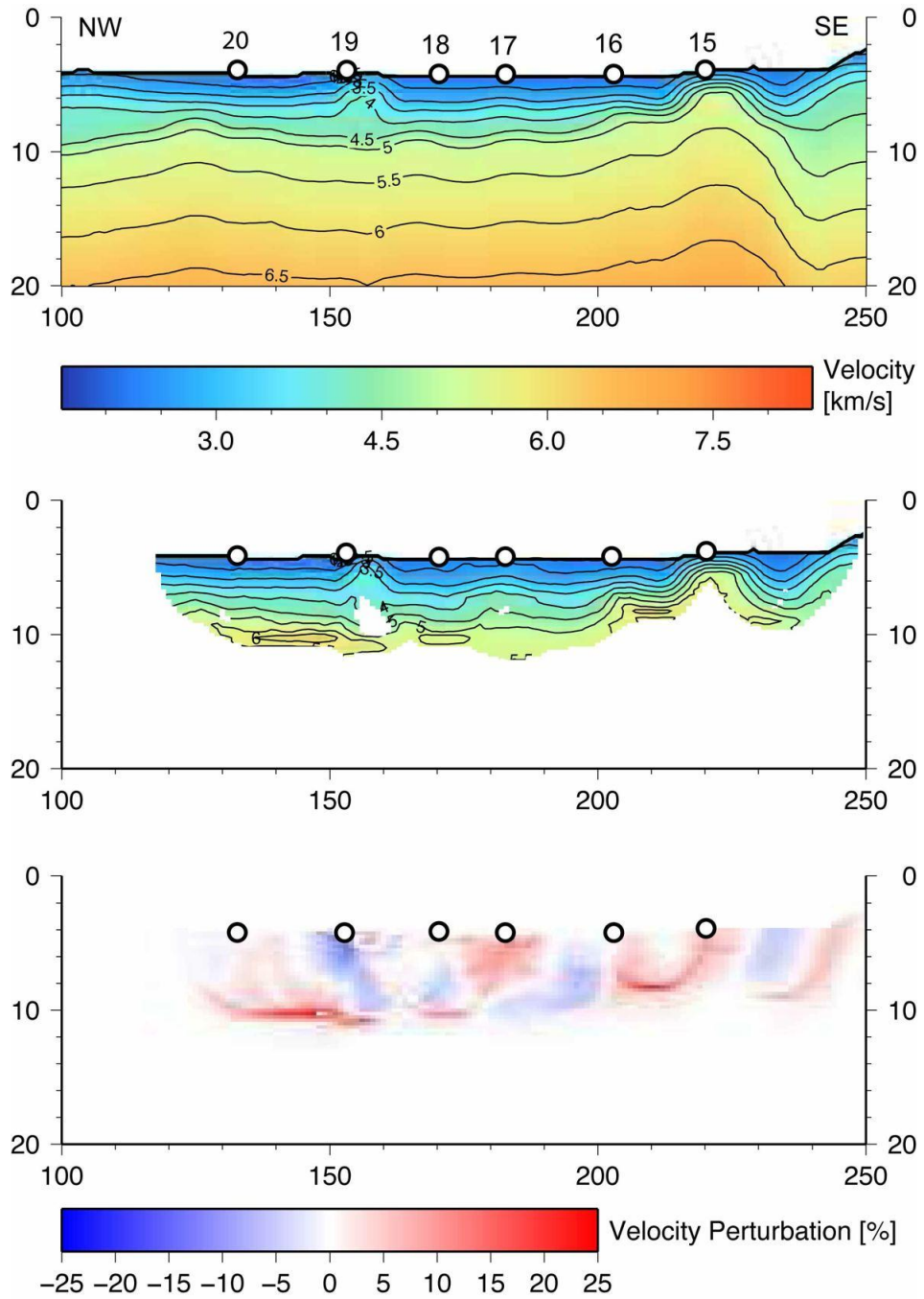


Figure 17: Line SISMAR05: Starting model (top), final model (middle) and difference between the final and initial models (bottom). White circles at the surface are the OBH and land stations. Too few PmP phases were identified to constrain properly a reflector at the base of the crust.

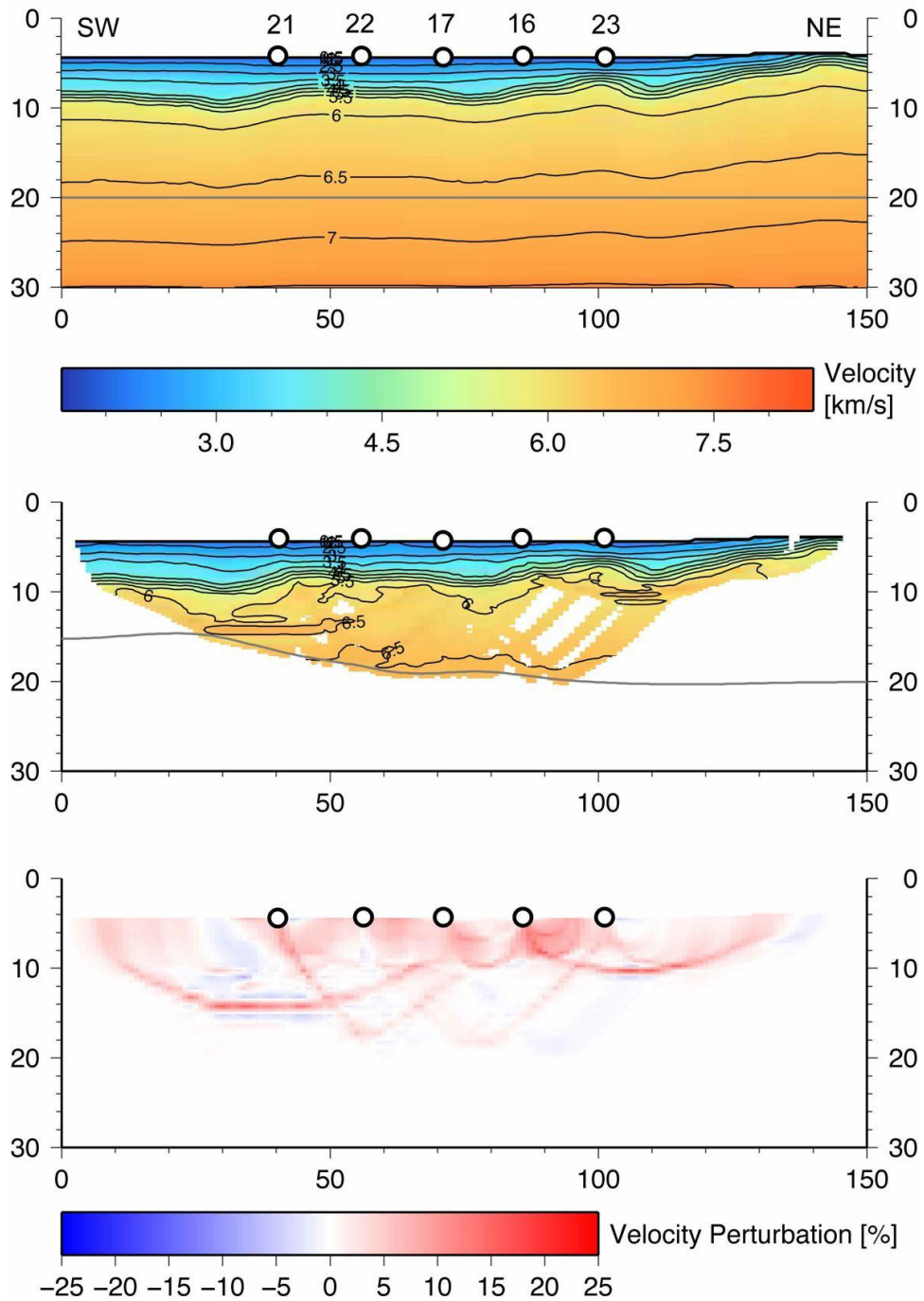


Figure 18: Line SISMAR08: Starting model (top), final model (middle) and difference between the final and initial models (bottom). White circles at the surface are the OBH and land stations. The gray line is the reflector at the base of the crust.

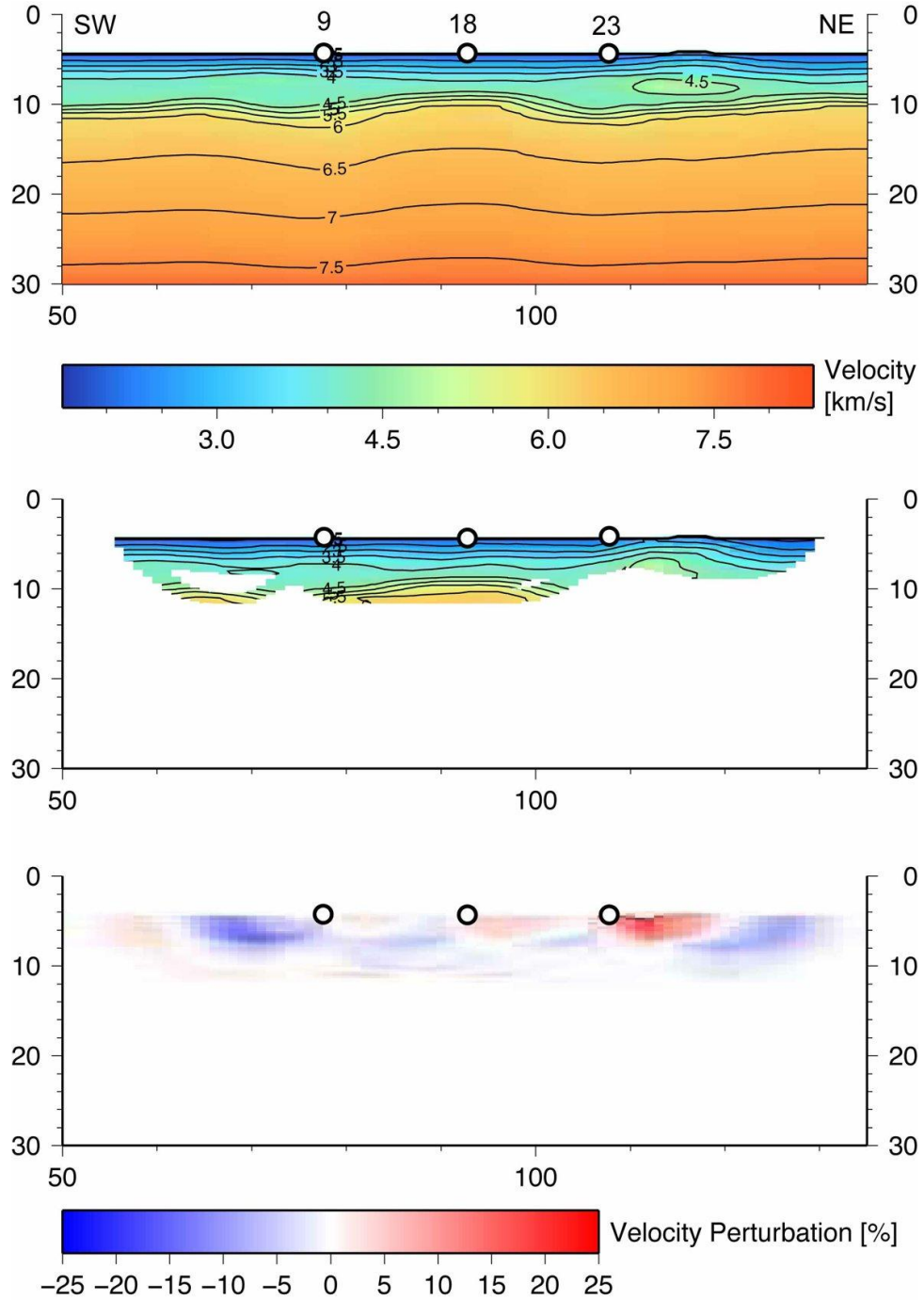


Figure 19: Line SISMAR10: Starting model (top), final model (middle) and difference between the final and initial models (bottom). White circles at the surface are the OBH and land stations.

These three profiles are characterized by a poor data quality. Line SISMAR08 compares well with the one published in Contrucci et al. (2004) both in the velocities and in the depth of the base of the crust. Along Lines SISMAR05 and 10, Jaffal et al. (2009) identified deep events (Pn phases) that we did not see in the present study. Consequently, the models of the present study are restricted to a shallower depth. One can argue on the complexity of Zelt models along

these three lines, considering the small amount of data and their less than fair quality. It may illustrate the hazard of hand-modeling (trial-and-error technique) favoring an over-interpretation of the data.

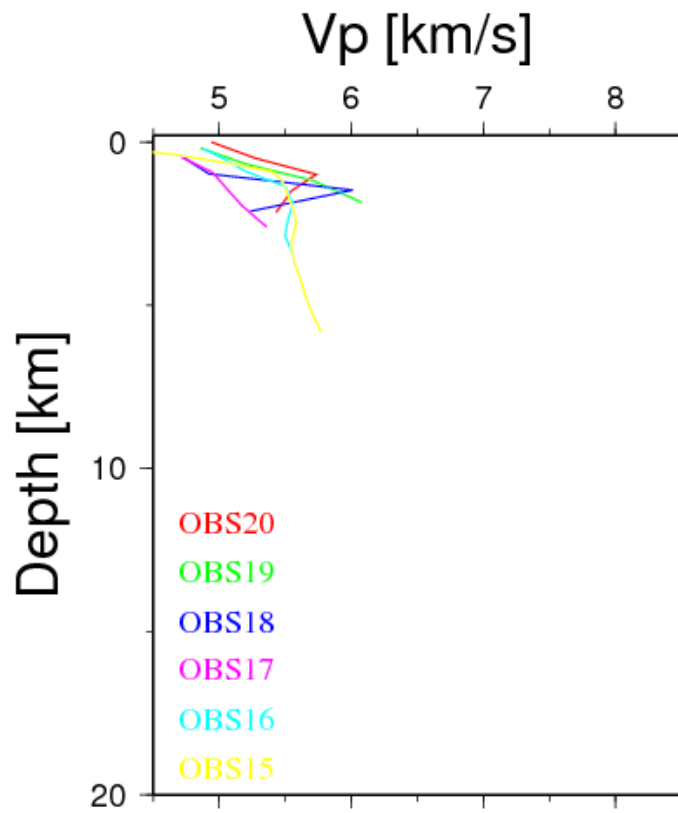


Figure 20: Line SISMAR05 1-D vertical velocity profiles below each OBH (continuous curves of various colors). The vertical axis indicates the depth below the top-basement, defined on the MCS profile.

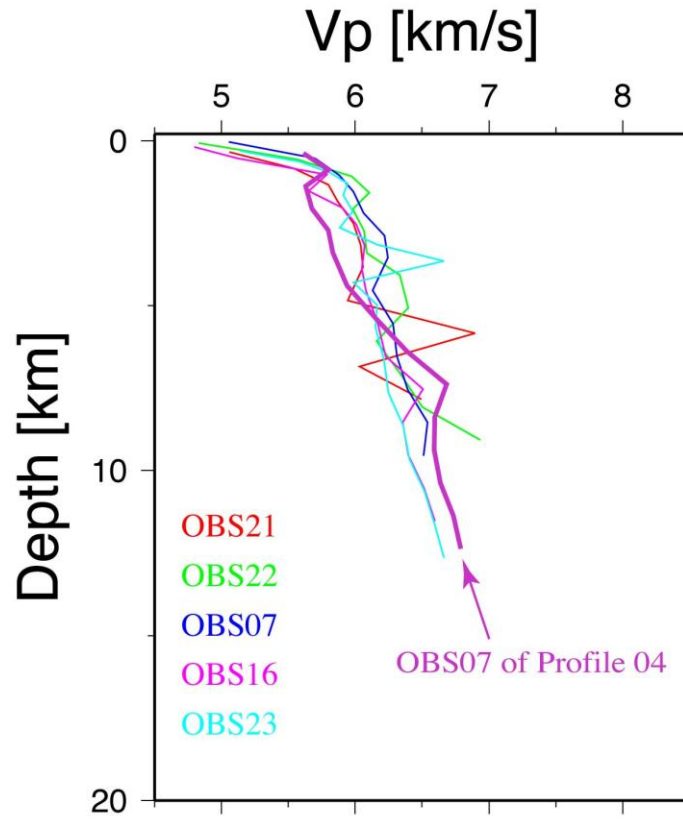


Figure 21: Line SISMAR08 1-D vertical velocity profiles below each OBH (continuous curves of various colors). The vertical axis indicates the depth below the top-basement, defined on the MCS profile. The thick violet curve is OBH07 along Line SISMAR04, to compare to the dark blue curve (same OBH07 but along Line SISMAR08).

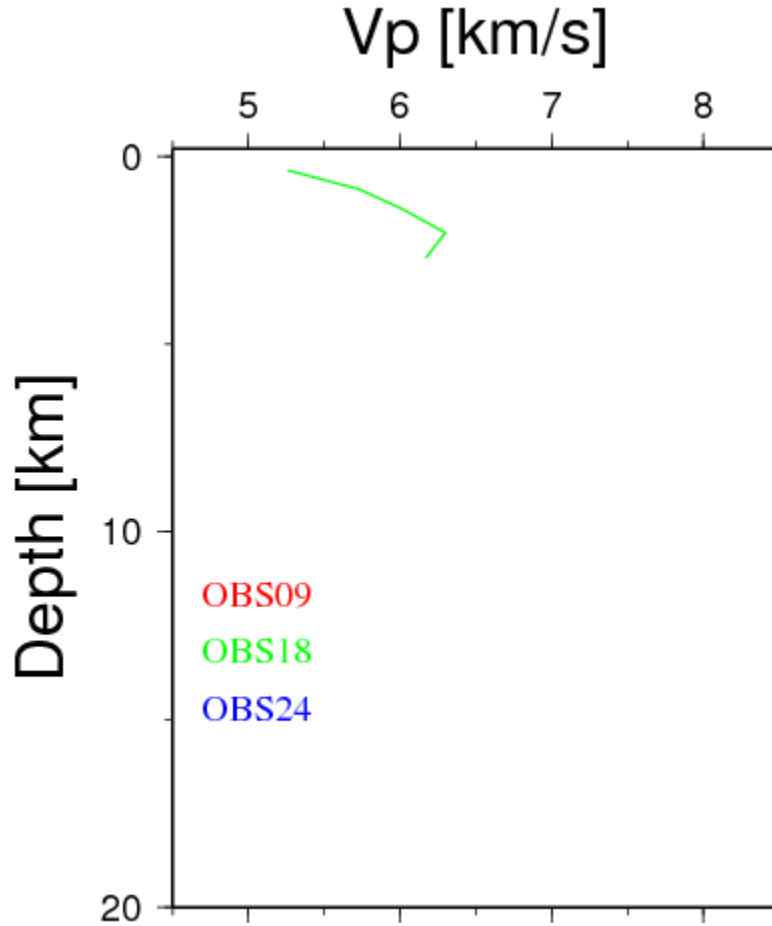


Figure 22: Line SISMAR10 1-D vertical velocity profiles below each OBH (continuous curves of various colors). The vertical axis indicates the depth below the top-basement, defined on the MCS profile.

Figure 20 and 22 present the 1-D vertical velocity profiles below the OBHs along the two lines SISMAR05 and 10. The very limited penetration of rays prevents from comparing from line to line. Along Line SISMAR08, the model after inversion reach the depth of 20 km and crustal velocities can be appropriately analysed (see Figure 21). First, velocity profiles along Line SISMAR08 show very limited variations, which is expected considering that the line is parallel to the strike of the margin. Second, the velocities at the intersection between Line SISMAR08 and 04 are relatively similar (OBH07, violet and dark blue curves, Figure 21). Compared to the averaged trend of the velocities along Line SISMAR08, the velocity in the crust below OBH07, inferred from the inversion of Line SISMAR04 data, shows rather lower values in the 5 first km below the basement and higher values beneath. These small differences can originate in the strong variability of velocities along Line SISMAR04 associated to the smoothing imposed to the model.

Interpretation of results

Previous interpretations

The continental affinity of the crust southeast of OBH07 is expressed by the velocity model with upper crustal velocities of 5.4 to 6.2 km/s (Contrucci et al., 2004) and the presence of typical tilted fault blocks beneath the continental slope. This is confirmed by DSDP holes (located in Figure 21), which penetrated granitic gneiss between OBH05 and 06 (Hinz et al., 1984). Magnetic lineation S1, the counterpart of the ECMA, is located near OBH12 on profile SISMAR04. S1 corresponds to the seaward edge of the salt domes (Maillard et al., 2006) and to the ocean-continent boundary defined from seismic velocities and magnetic anomalies (Hinz et al., 1982; Roeser et al., 2002). Contrucci et al. (2004) interpret crustal velocities below OBH13 and 14 as typical for oceanic crust.

If there is no doubt for Contrucci et al. (2004) about the presence of thinned continental crust southeast of OBS07 and of typical oceanic crust northwest of OBH12, however, there is a uncertainty about the nature of the crust between OBH07 and 12, over a distance of about 80 km. Contrucci et al. (2004) only stated that this transitional domain does not display high lower crustal velocities associated with serpentinized upper mantle (as shown in Figure 10 left) typically found in the transitional domains of non-volcanic margins.

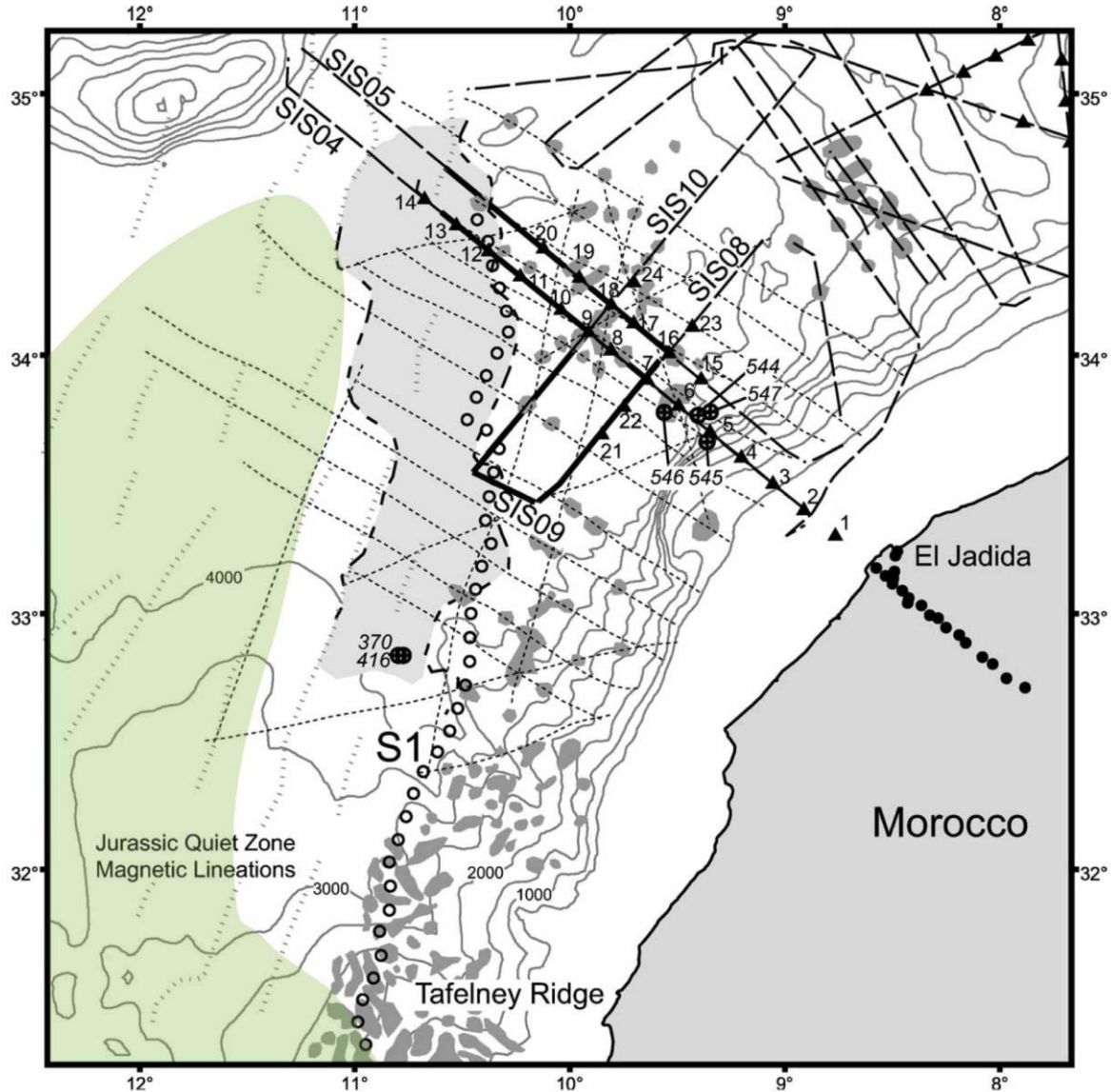


Figure 23: Location of the S1 magnetic lineation (open dots) and salt diapirs (small grey polygons), mostly located landward of S1 (Maillard et al., 2006). DSDP holes are indicated. In light green, the extent of unusually high lower crustal velocities from sonobuoy data (Holik et al., 1991).

Four Sismar MCS lines are crossing S1 (Figure 23). Profiles SIS09 and SIS10 (Figure 24) show a landward dipping reflector (LDR) overlain by a ~ 0.5 sec layered unit (LU). No mantle reflections are identified. The LDR plunges toward the northeast, below the thinned continental crust (Maillard et al., 2006). The location where the LDR and LU are reaching the top of the basement is located in the close vicinity of S1. Sediments of the deep margin overlap LU oceanwards. At depth, the LDR may reach the Moho level but no clear relationship between the LDR and the Moho can be established. From profile SIS08 (not shown here), Maillard et al. (2009) suggest that the LDR seems to penetrate at mantle depth. On SIS04, only weak landward dipping reflections may suggest the occurrence of a LDR starting from S1 location

down to a depth of ~1 sec in the basement. The LDR dips 6°-7° northeastwards, which is not the expected tensional direction prior to S1.

Maillard et al. (2009) interpret the LDR as a large fault, which seems to cut the Moho and then could be a lithospheric detachment which may have been active later than the Triassic - early Liassic rifting. For Maillard et al. (2009), the material below the LDR would be exhumed mantle with a low 50 to 60% serpentinization rate explaining the 6 - 6.5 km/s velocity (Figure 10). They interpreted the LU as magmatic material and lavas possibly originated from asthenospheric melted material rising from the lower extremity of the LDR and guided along it to the surface of the basement.

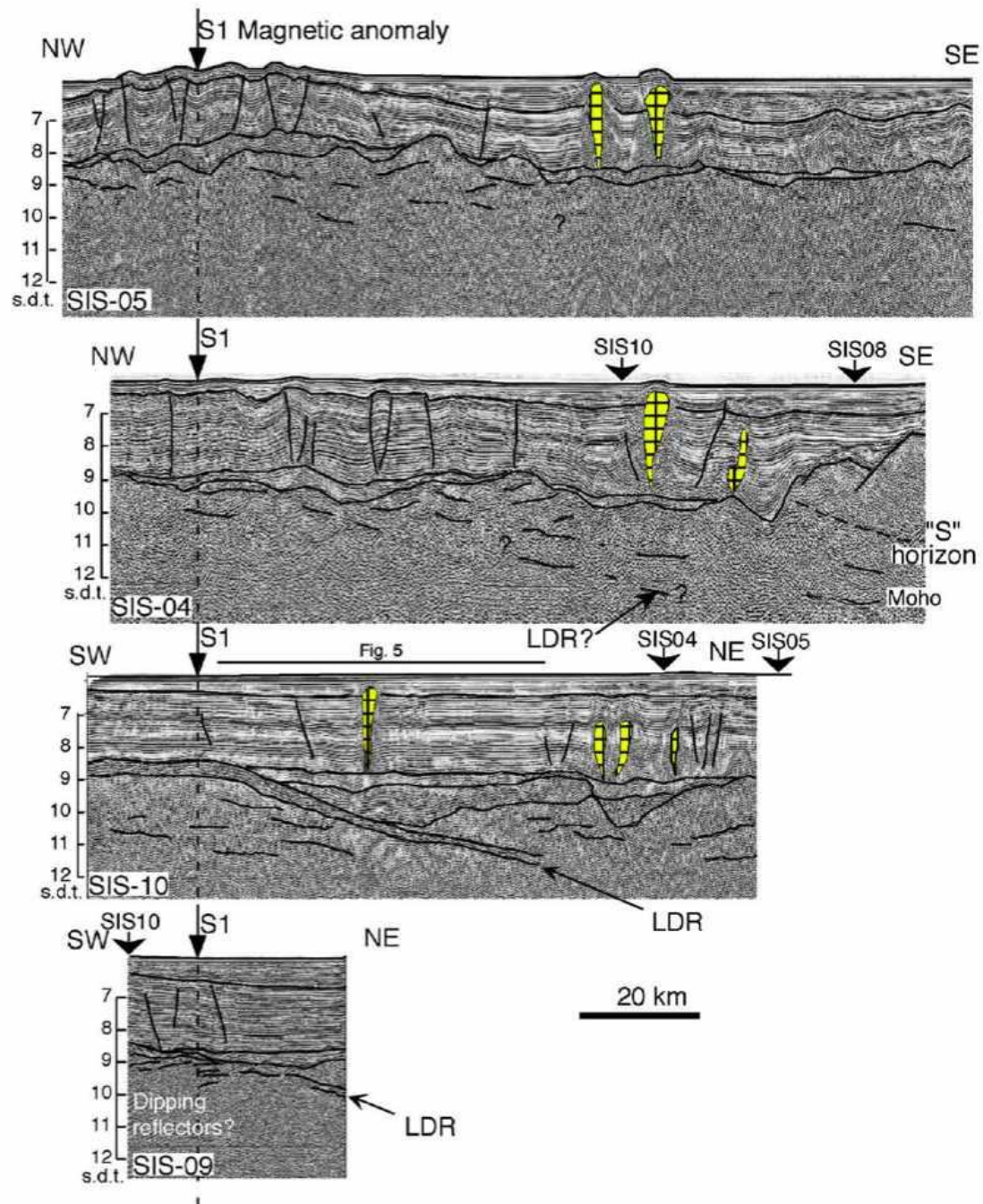


Figure 24: The four SISMAR MCS profiles are aligned with respect to S1 located in Figure 23. The landward dipping reflector (LDR) is identified on SIS10 and 09, but not on profiles SIS04 and 05 where only crustal reflections are dipping in the same direction (Maillard et al., 2006). Above the LDR, the layerd unit (LU) is ~0.5 second thick.

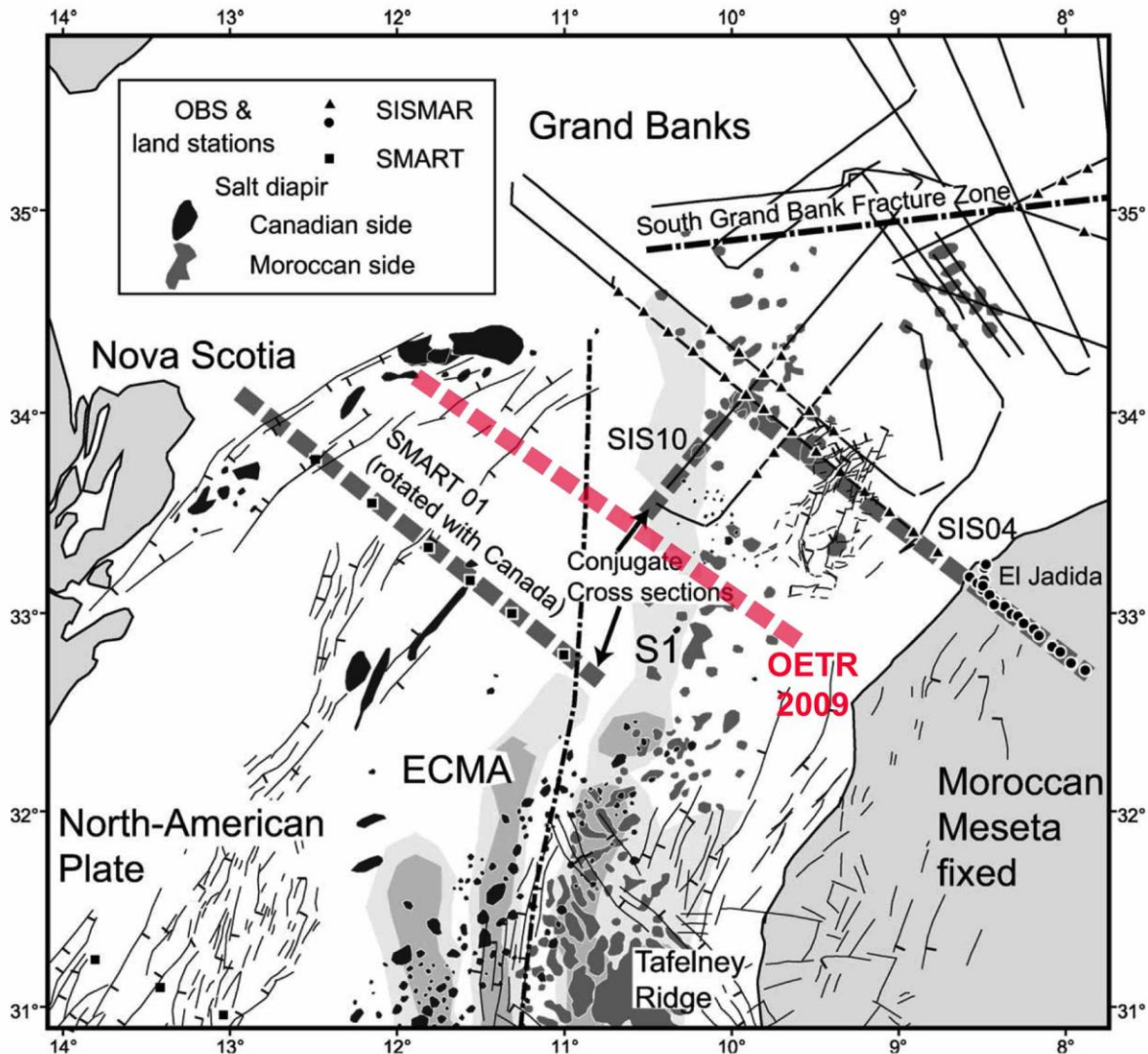


Figure 25: Plate reconstruction between Morocco and Nova Scotia (Sahabi et al., 2004) separated by the stippled-dashed line, at the time of juxtaposition of magnetic lineations S1 and ECMA. Conjugate profiles are built on SIS04 and SMART01 (black squares) (Figure 26) and on SIS04 and OETR2009 (red squares) (Figures 29 and 30).

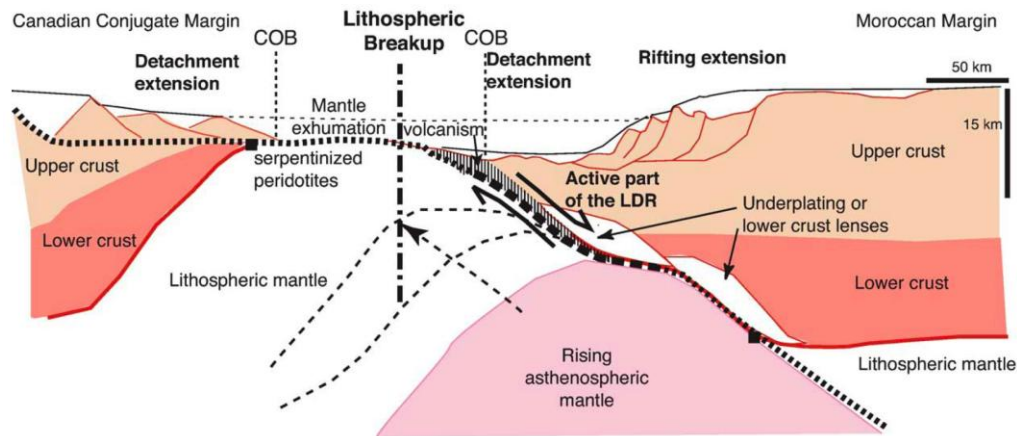


Figure 26: 2-D model of the conjugate margins of the Morocco and Nova Scotia margins based on SIS04 and SMART01 lines.

On the Canadian side, a 150-km-wide transition zone is observed on SMART01 profile with a 5-km-thick lower layer (7.2 - 7.6 km/s) interpreted as partially serpentinized mantle (Funck et al., 2004). At its landward extremity, this layer is overlain by highly altered continental crust (5.4 km/s) extending up to the seaward limit of the Jurassic salt province. Farther seaward, the upper layer is interpreted as exhumed and highly serpentinized mantle (5.1 km/s) separated from the lower layer by sub-horizontal reflectivity, which probably represents a serpentinization front. To the east, the oceanic crustal thickness is 4 km with layer 2 velocities of 4.6 - 5.0 km/s. Layer 3 velocities of 6.4 - 6.55 km/s are lower than typical lower oceanic crust velocities but consistent with a low magma supply and increased tectonism as observed on the reflection profile.

Figure 26 shows the SIS04-SMART01 2-D model of Maillard et al. (2006), which does not consist of true conjugate profiles, as the two conjugate sections are ~170 km apart (Figure 25). Assuming that the lack of conjugacy is overcome by the 2 dimensionality of the conjugate margins, they proposed a rifting episode in two stages: a widespread crustal extensional stage followed by the exhumation of the lower continental crust and mantle through the play of a large detachment surface as suggested by Whitmarsh et al. (2001).

Interpretation of SISMAR04 Line

To understand how formed and evolved one of the oldest continental margins in the world, we have first to constrain the interpretation of the velocity structure of the transitional domain on SISMAR04 Line. Figure 27 summarizes the crustal velocity profiles beneath each OBS obtained by different methods. They present similarities, complementarities and differences.

As they are clearly outside the oceanic crust patches (Figure 27) on all the three graphs, OBH08 and 09 are located above thinned continental crust, even if the crust between 170 and 210 km is sparsely covered, implying a lower resolution. Thus, the continental crust and thinned continental crust extends at least from OBH01 to OBH09 ($x > 175$ km).

The 7.2 to 7.5 km/s velocities observed below OBH11 (Figures 27b and c) at 14 km depth may extend to OBH13 on the detailed processing performed on the transitional crust

(Figure 12). A reasonable interpretation of these high velocities is to assume that the lower part of the crust consists of serpentinized mantle. Above this body, between OBH12 to 14, the nature of the crust might be either lower continental crust or highly serpentinized mantle. Though there is no definitive argument to prefer one alternative or the other, we prefer the existence of lower continental crust for the following reason: the 6.5 km/s iso-value curve moves obliquely 5 km upwards from beneath OBH08 and 09 to OBH12 and 13 (Figure 28), defining an oblique boundary between domains A (thinned continental crust) and B (serpentinized mantle obliquely overlain by lower continental mantle?). In addition, this boundary corresponds exactly to the LDR identified on MCS profiles, reconciling the results of the MCS (Figure 24) and WAS data.

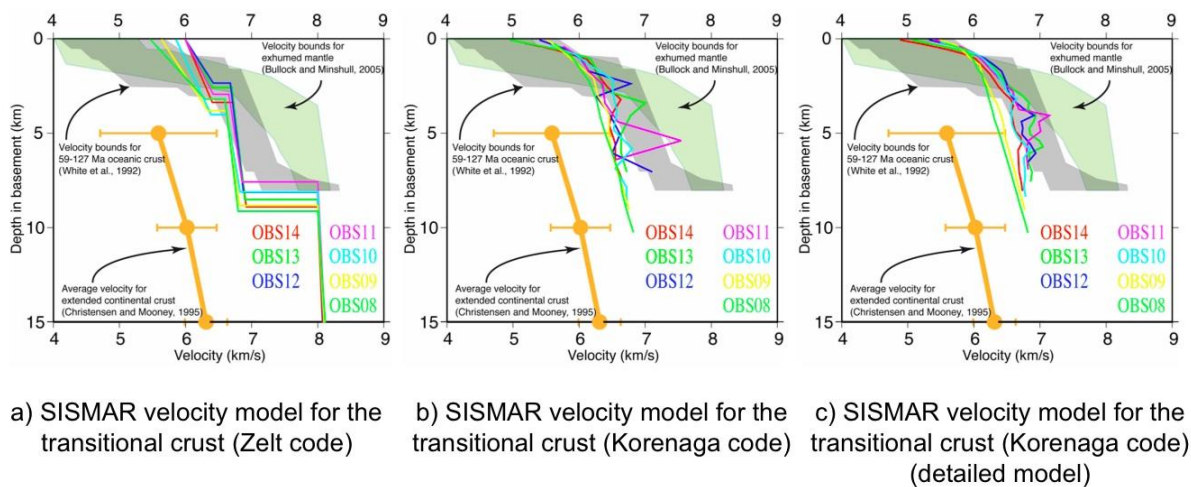


Figure 27: Close-up of figures 10 and 13 where only vertical profiles in the transitional crust are shown.

Contrucci et al. (2004) interpret crustal velocities below OBH13 and 14 as “more” typical of oceanic crust. This is not so clear from their velocities (Figure 27a) because 1) the crust beneath OBH13 and 14 is thicker than normal and 2) velocities are either on the extreme left-hand side of the oceanic crust patch or lower than normal at depths deeper than 5 km below basement. This analysis is also confirmed by the velocity models of Figure 27b, where the velocity trend of OBH14 is very different from others. Below a depth of 3 km, velocity values are outside and on the lower velocity side of the oceanic crust patch. As OBH14 is located on the flank of Coral Patch Seamount, in an area where the crust is thickening, the crust beneath OBH14 might be related to the nature of the abnormal thick Coral Patch crust. If this is true, the westernmost extremity of the SISMAR04 profile would not be representative of the conjugate portion of OETR2009 Profile.

If velocities of OBH14 are not representative of the surrounding area, what will be the expected nature of the crust, especially ~100 km southwestwards of OBH14, in the area where the conjugate portion of OETR2009 is located (Figure 25)? In 1991, Holik et al. identified an area roughly corresponding to the Canary swell, with high lower crustal velocities (7.1-7.4 km/s)

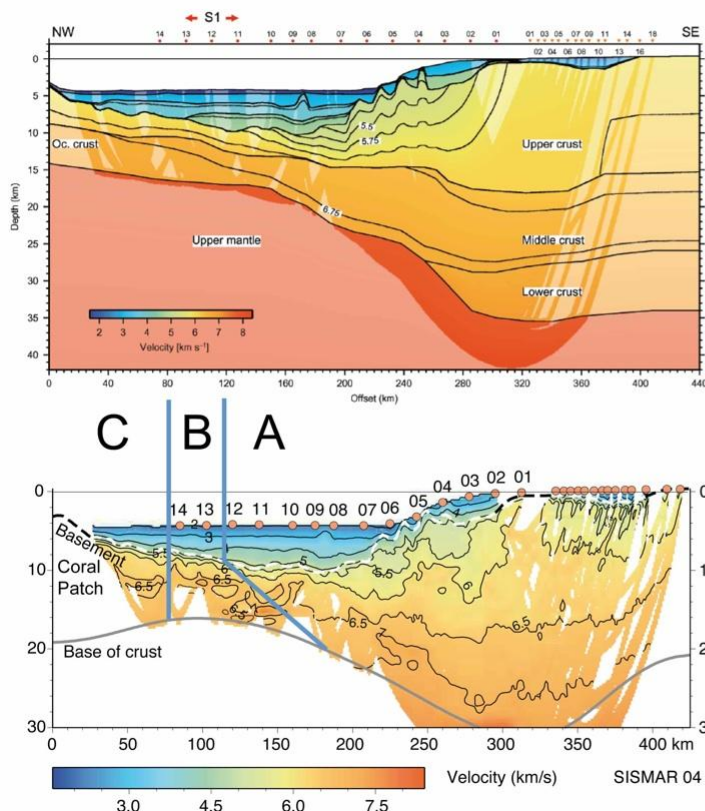
(Figure 23). The thickness of the high lower crustal body is 2 to 4 km and was interpreted as underplating linked to the Canary thermal anomaly. However, there are no data north of 34.6°N and as the seafloor spreading rate between ECMA and Blake Spur magnetic anomaly (BSMA) is 0.5 cm/yr and symmetrical in between on both sides of the Atlantic, seafloor spreading mantle accretion might be also considered as a significant alternative.

To conclude, the shape of layers given by Contrucci et al. (2004) using the Zelt code (Figure 28) does not reflect both the existence of serpentinized mantle velocities at the base of the transitional crust, and the existence of LDRs on MCS profiles. The proposed model based on this study (using the Korenaga code) is very simple (Figure 28, domains A, B and C):

A) the continental crust thins from the shelf to OBH09 and then progressively disappears from OBH09 to 12, above a major detachment fault (LDR) identified both on MCS profiles and in this study (upper plate).

B) the lower plate consists of serpentinized mantle at its base overlain by possible lower crust (or exhumed mantle). In that case, the relative motion along the detachment fault would be only a few tens of kilometers. If the upper part of the crust consists of highly serpentinized crust, then the motion along the detachment fault might exceed 100 km. In this report, we favor the first hypothesis.

C) the western extremity of SISMAR04 is located on the flank of Coral Patch Seamount, suggesting that OBH13 and 14 are not representative of the crust west of magnetic lineation S1. Old sonobuoy data suggest that the crust consists of serpentinized mantle, as found on OETR2009 Profile.



A

- Thinned continental crust

B

- Serpentinized mantle
at the base of the crust?
- Lower cont. crust above?

- Exhumed cont. mantle?

C

- Seafloor spreading mantle?
- Coral Patch abnormal crust?

Figure 28: Comparison between the Contrucci et al. (2004) velocity model (top) and the tomographic model (top), with similar color scale and iso-value contours for proper comparison.

Nova Scotia-Morocco conjugate velocity profiles: First observations

Figures 29 and 30 show reconstructions of velocity profiles SISMAR04 and OETR2009 at the time of conjugate magnetic anomalies ECMA/S1 (195 Ma, latest Triassic) and E (175 Ma, Middle Jurassic, Aalenian). Note from the ECMA/S1 plate reconstruction (Figure 25) that profiles SISMAR04 and OETR2009 are laterally offset of ~100 km. In addition, as previously mentioned, the western extremity of Profile SISMAR04 is located on the flank of Coral Patch Seamount, which means that the westernmost end of the SISMAR04 velocity profile cannot be used as it stands in the 175 Ma conjugate reconstructed profile of Figure 30.

Based on conjugate velocity profiles of Figures 29 and 30, Figure 31 shows our final interpretation. The interpretation at the time of ECMA/S1 is based on our interpretation of SISMAR04 Profile and on OETR2009 Makris preliminary interpretation (personal communication, 2010) (Figure 28). The interpretation at 175 Ma is based on our interpretation of SISMAR04 profile with the hypothesis that west of S1, the crust consists of serpentinized mantle as well as on OETR2009 Makris preliminary interpretation (personal communication, 2010) (Figure 29), where a 90-km long, 4-5 km thick body has been identified at the base of the crust. Velocities of 7.2 to 7.5 km/s suggest that this body is serpentinized mantle. On top of it, a 2-3 km thick layer with velocities of 5.3 km/s clearly corresponds to a layer of highly serpentinized mantle, whose top coincides with the hummocky basement on the coincident MCS profile. The crust in between ECMA/S1 and 175 Ma might be either exhumed mantle from beneath the adjacent continents, or oceanic serpentinized mantle. It is extremely difficult to decipher between these two hypotheses (see numerous discussions concerning the origin of the serpentinized mantle between Iberia and Newfoundland). However, several arguments favor a formation of the ECMA/S1 to 175 Ma crust by seafloor spreading:

- 1) The contact of the 6-km thick serpentinized body with the lower/upper continental crust on Profile OETR2009 is almost vertical. With such a geometry of the interface, it seems difficult to emplace this serpentinized body by the exhumation process.
- 2) On the SISMAR04 MCS profile, from S1 to the flank of Coral Patch Seamount (over a distance of 110 km), the deep sediment layers regularly onlap westward on top of the basement, sediments becoming younger and younger to the west. Consequently, since chron ECMA/S1, the acoustic basement is younger to the west and mantle exhumation from ECMA/S1 location is not supported. In the case of mantle exhumation, the basement would have been younger from west to east and sediments would have been younger eastwards.
- 3) From kinematic considerations, which will be explored in more detail in the near future, the Central Atlantic opening (or extension if no oceanic crust was formed) seems to be almost symmetrical since chron ECMA/S1. A simultaneous exhumation process from beneath the two margins seems to be extremely difficult to imagine, though this process was mentioned for the Iberia/Newfoundland margins.

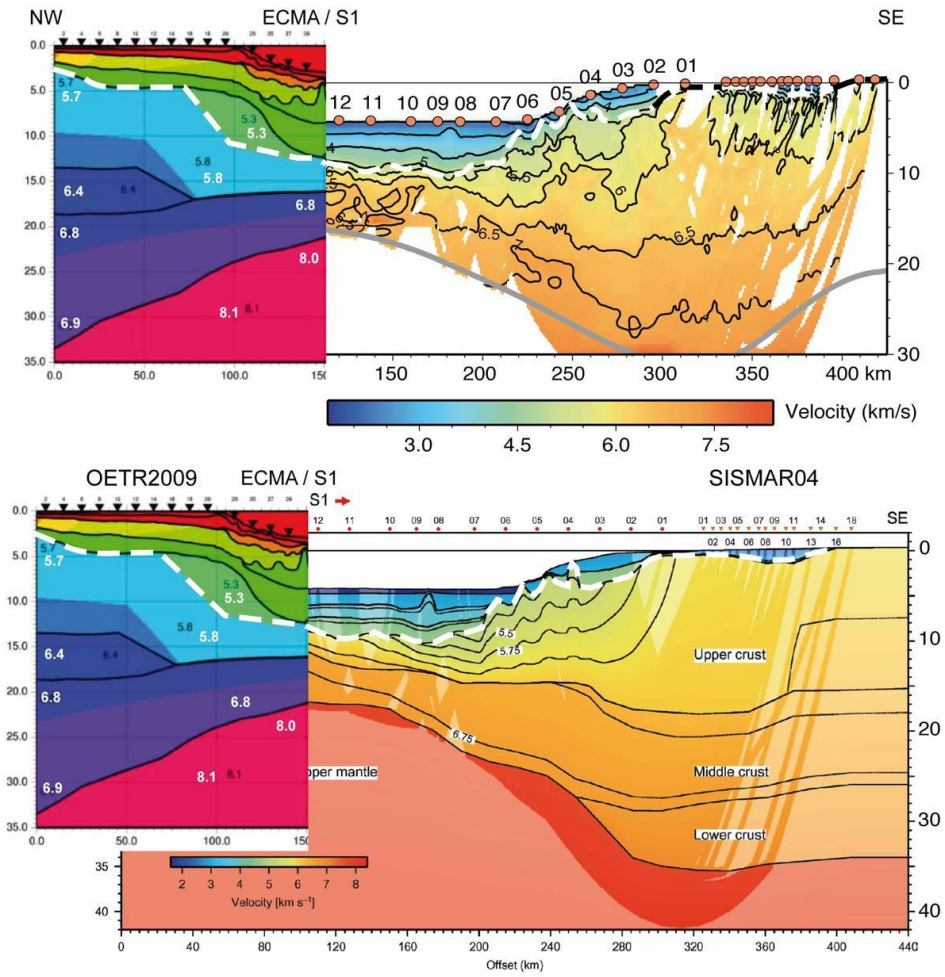


Figure 29: Conjugate velocity profiles SISMAR04 and OETR2009 with the two types of interpretations (Zelt (bottom) and Korenaga (top) codes) at the time of anomalies ECMA/S1. Preliminary interpretation of Profile OETR2009 from Makris et al. (personal communication, 2010). As the sediment thickness is double on the Nova Scotia side compared to the Moroccan side, Profile OETR2009 has been moved upwards in order to show crustal coincidence.

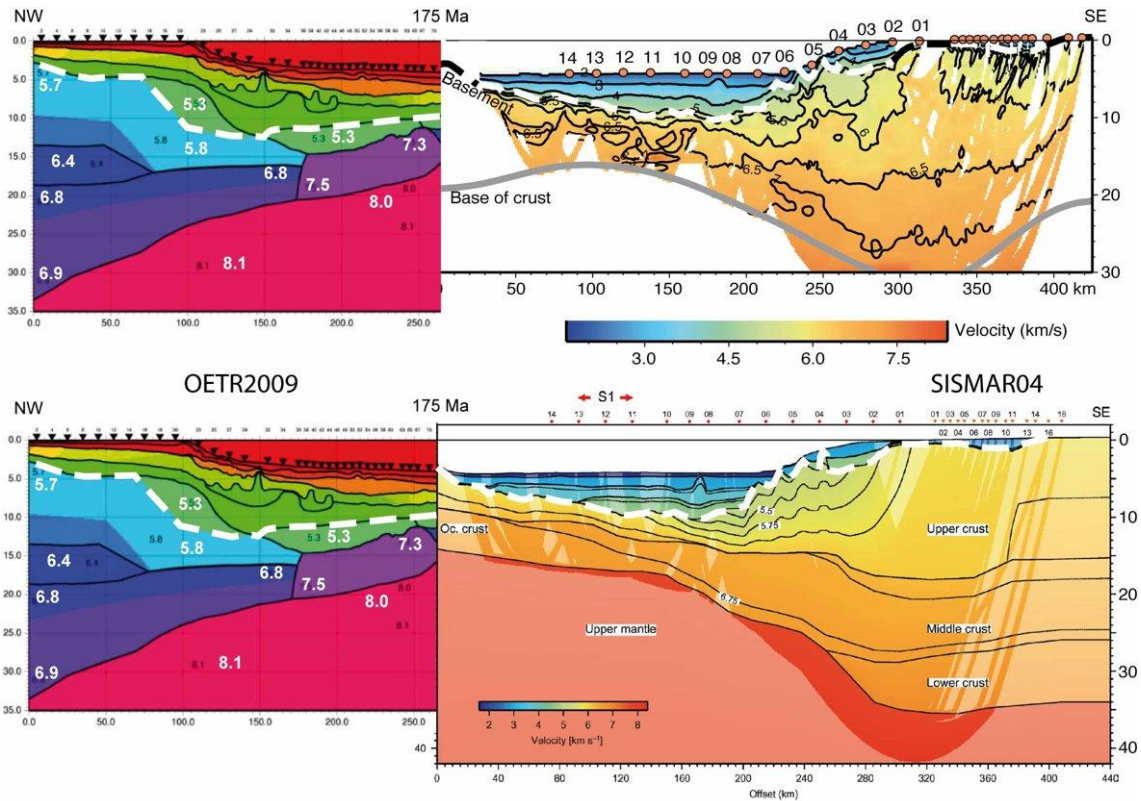


Figure 30: Conjugate velocity profiles SISMAR04 and OETR2009 with the two types of interpretations (Zelt (bottom) and Korenaga (top) codes) at the time of anomalies E (175 Ma). Preliminary interpretation of Profile OETR2009 from Makris et al. (personal communication, 2010).

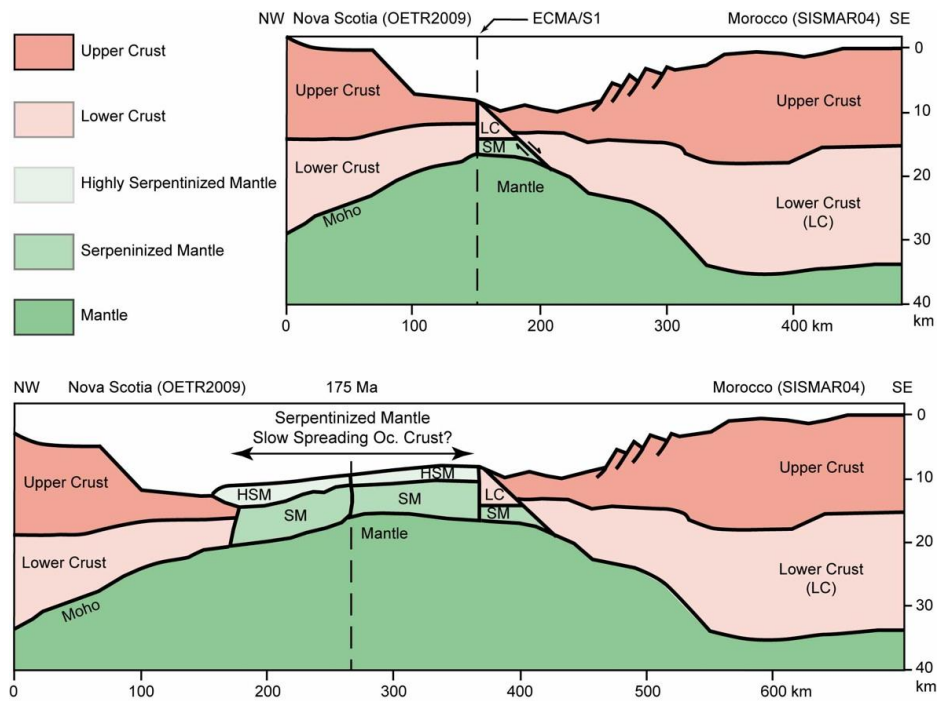


Figure 31: Crustal interpretation of conjugate velocity profiles SISMAR04 and OETR2009 at the time of anomalies ECMA/S1 and E (175 Ma) without syn- and postrift sediments. SM, serpentinized mantle; HSM, highly serpentinized mantle.

Scheme of formation and evolution of the Nova Scotia/Morocco conjugate margins

From previous observations, we can propose a scheme of formation and evolution of the Nova Scotia/Morocco conjugate margins in three stages (Figure 32):

1) During the first phase of rifting (late Triassic), ending at the time of emplacement of the ECMA/S1 magnetic anomalies (~195 Ma), the continental crust thinned, probably by pure shear, as established for the large majority of passive continental margins (e.g. Sibuet, 1987, Lavier and Manatschal, 2006). Note that at the end of this first phase of extension, the two margins were asymmetrical (Figure 32a). The Moroccan margin is much wider than the Nova Scotia margin: 110 km between the axis of S1 and the African coast in the prolongation of the rotated SMART01 Profile (Figure 25) and 200 km between the axis of S1 and the African coast along SISMAR04 Profile. Do we have some asymmetry in the extensional process or some rift jump during or at the end of the first rifting phase?

2) During the second phase of rifting (195 Ma to 175 Ma), first the LDR initiated right at the beginning of the second rifting phase. About 20 km of lower plate was extracted from beneath the Moroccan margin (Figure 32b). With a full spreading rate of 1 cm/yr between ECMA/S1 (~195 Ma) and BSMA (~165 Ma), the extraction of 20 km of lower plate lasted on the order of 2 Ma, bringing the lower crust belonging to the lower plate close to the sea-bottom. Serpentinization of the uplifted mantle probably occurred with sea-water channeling down through the LDR. Second, the asthenospheric mantle (and not oceanic crust) raised to the sea-bottom, due to a combination of several factors: cold lithosphere, cold margin and slow spreading rate (Figure 32c). About 200 km of serpentinized mantle was emplaced by sea-floor spreading. An alternative scenario would consist in the prolonged exhumation of mantle from beneath the Moroccan margin or from beneath both margins. However, as previously seen, there is no depositional sedimentary features associated with such exhumation process on MCS profiles.

3) Since 175 Ma, typical oceanic crust was emplaced by sea-floor spreading, as evidenced on Profile OETR2009 (Makris, personal communication, 2010), which shows 130 km of typical oceanic crust emplaced east of the serpentinized body (Figure 32d).

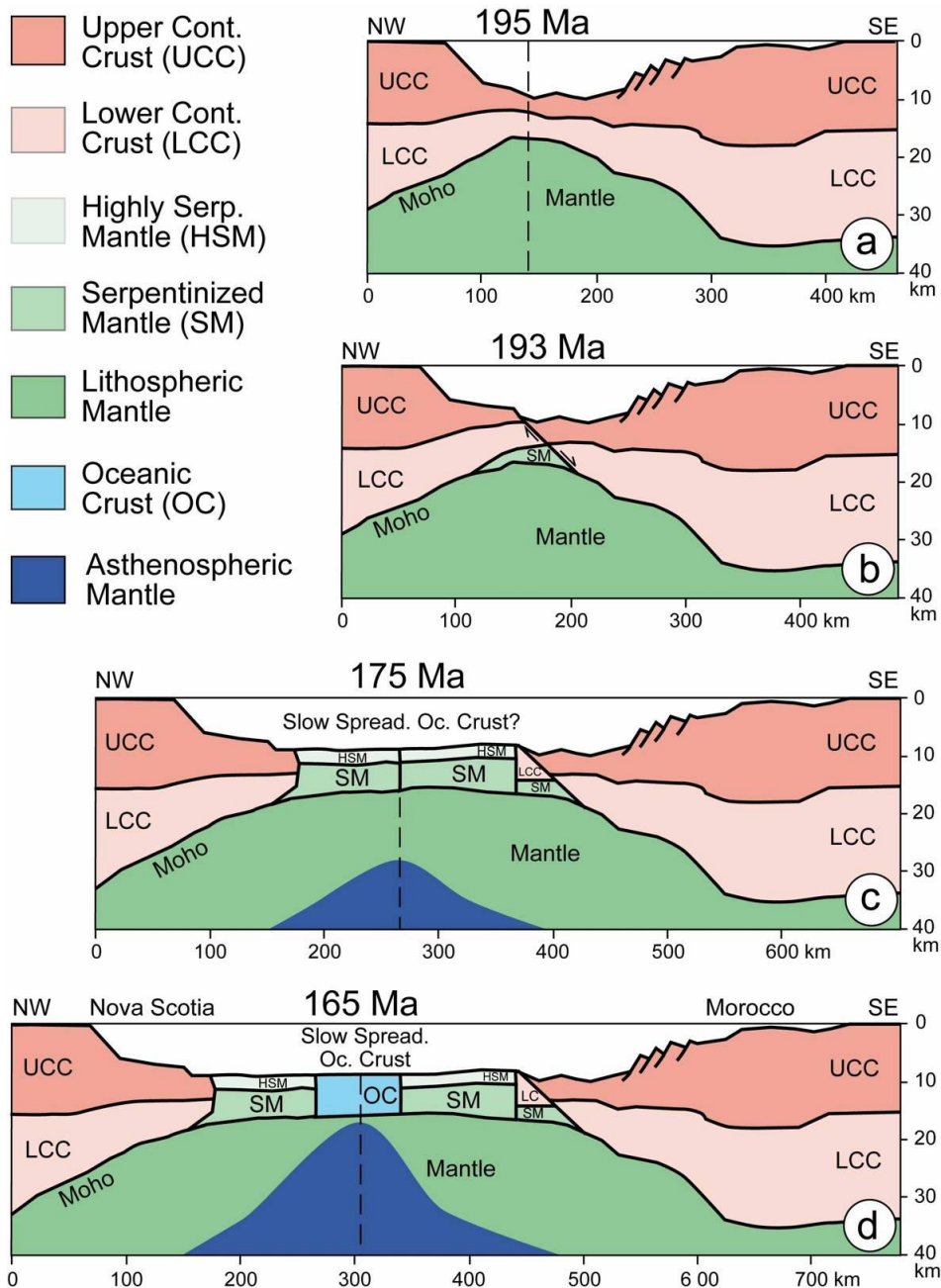


Figure 32: Scheme of formation and evolution of the Nova Scotia/Morocco conjugate margins. a) At the end of the first rifting phase (chron ECMA/S1, 195 Ma). b) After 20 km of lower plate exhumation along the LDR (193 Ma). c) At the end of the second rifting phase (chron E, 175 Ma). d) During the accretion of typical oceanic crust (chron BSMA, 165 Ma).

References

- Bullock A.D. and Minshull T.A., 2005. **From continental extension to seafloor spreading: Crustal structure of the Goban Spur rifted margin, southwest of the UK**, *Geophys. J. Int.*, 163, 527–546.
- Contrucci I., Klingelhoefer F., Perrot J., Bartolome R., Gutscher M.-A., Sahabi M., Malod J. and Réhault J.-P., 2004. **The crustal structure of the NW Moroccan continental margin from wide-angle and reflection seismic data**, *Geophys. J. Int.*, 159, 117–128.
- Christensen N. I. and Mooney W. D., 1995. **Seismic velocity structure and composition of the continental crust: A global view**, *J. Geophys. Res.*, 100(B6), 9761–9788, doi:10.1029/95JB00259.
- Funck T., Jackson H.R., Loudon K.E., Dehler S.A. and Wu Y., 2004. **Crustal structure of the northern Nova Scotia rifted continental margin (eastern Canada)**, *J. Geophys. Res.*, 109, B09102, doi:10.1029/2004JB003008.
- Hinz K., Winterer E.L. et al., 1984. Initial Reports DSDP 79, U.S. Government Printing Office, Washington D.C., 934 pp.
- Hinz K., Dostmann, H. and Fritsch, J., 1982. **The continental margin of Morocco: Seismic sequences, structural elements and geological development**, in *Geology of the Northwest African continental margin*, eds K. H. von Rad et al., Springer Verlag, Berlin, pp. 34–60.
- Holik J.S., Rabinowitz P.D. and Austin J.A., 1991. **Effects of the Canary hotspot volcanism on the structure of oceanic crust off Morocco**, *J. Geophys. Res.*, 96, 12,039–12,067.
- Jaffal M., Klingelhoefer F., Matias L., Teixeira F. and Amrhar M., 2009. **Crustal structure of the NW Moroccan margin from deep seismic data (SISMAR Cruise)**, *C. R. Geoscience* 341, 495–503.
- Korenaga J., Holbrook W.S., Kent, G.M., Kelemen P.B., Detrick R.S., Larsen, H.-C. Hopper J.R. and Dahl-Jensen T., 2000. **Crustal structure of the Southeast Greenland margin from joint refraction and reflection seismic tomography**, *J. Geophys. Res.*, 105, 21,591–21,614.
- Lavier, L.L. and Manatschal G., 2006, **A mechanism to thin the continental lithosphere at magma-poor margins**, *Nature*, 440, 324–328, doi:10.1038/nature04608.
- Maillard A., Malod J., Thiebot E., Klingelhoefer F. and Réhault J.-P., 2006. **Imaging a lithospheric detachment at the continent–ocean crustal transition off Morocco**, *Earth and Planet. Sci. Lett.*, 241, 686–698.
- Roeser H., Steiner C., Schreckenberger B. and Block M., 2002. **Structural development of the Jurassic Quiet Magnetic Zone off Morocco and identification of Middle Jurassic magnetic lineations**, *J. Geophys. Res.*, 107, B10, 2207, doi:10.1029/2000JB000094.
- Sahabi M., Aslanian D. and Olivet J.-L., 2004. **Un nouveau point de départ pour l'histoire de l'Atlantique central**, *C. R. Acad. Sci. Paris*, 336, 1041–1052.
- Sibuet J.-C., 1987. **Contribution à l'étude des mécanismes de formation des marges continentales passives**, Thèse de Doctorat d'Etat, Université de Bretagne Occidentale, Brest, 351 p.
- White R.S., 1992. **Crustal structure of North Atlantic continental margins**, *J. Geol. Soc. London*, 149, 841–854.
- Whitmarsh R.B., Manatschal G. and Minshull T.A., 2001. **Evolution of the magma-poor continental margins from rifting to seafloor spreading**, *Nature*, 413, 150–154.

Zelt, C.A. and Smith R.B., 1992. **Seismic traveltime inversion for 2-D crustal velocity structure**, Geophys. J. Int., 108, 16-34.